

## **Development of the Amyloid Fibril Characterisation Toolbox**

New use for old dyes

DAVID LINDBERG

*Department of Biology and Biological Engineering*

CHALMERS UNIVERSITY OF TECHNOLOGY  
Göteborg, Sweden 2015



THESIS FOR THE DEGREE OF LICENTIATE OF ENGINEERING

Development of the Amyloid Fibril Characterisation  
Toolbox

New use for old dyes

DAVID J. LINDBERG

Department of Biology and Biological Engineering

CHALMERS UNIVERSITY OF TECHNOLOGY

Gothenburg, Sweden 2015

Development of the Amyloid Fibril Characterisation Toolbox  
New use for old dyes  
DAVID J. LINDBERG

© DAVID J. LINDBERG, 2015.

Department of Biology and Biological Engineering  
Chalmers University of Technology  
SE-412 96 Gothenburg  
Sweden  
Telephone + 46 (0)31-772 1000

Cover:

[Top left: Illustration showing the repetitive cross- $\beta$  structure of an amyloid- $\beta$  protofilament. Adapted from Luhrs et al [37]. Top right: Atomic force microscopy image of amyloid- $\beta$  fibrils deposited on a glass surface. Bottom: Chemical structure of the two dyes used in this thesis, YOYO-1 (top) and thioflavin-T (bottom).]

[Department of Biology and Biological Engineering]  
Gothenburg, Sweden 2015

Development of the Amyloid Fibril Characterisation  
Toolbox  
New use for old dyes

DAVID J. LINDBERG

Department of Biology and Biological Engineering

CHALMERS UNIVERSITY OF TECHNOLOGY

**ABSTRACT** Amyloid fibrils are self-assembled protein homopolymers that play central roles in the pathology of several human diseases, most notably in progressive neurodegenerative diseases such as Alzheimer's disease (AD). In AD, fibrils are formed by the amyloid- $\beta$  ( $A\beta$ ) peptide, an enzymatic cleavage product that is naturally produced in human brain tissue. The fibrillar  $A\beta$  accumulates in deposits known as senile plaques in the diseased AD brain, and the processes by which this occurs are postulated to be primary causes of the neuronal loss that is associated with AD progression. As such, it is of great importance to understand how  $A\beta$  fibrils are formed, and why they exert neurotoxic effects in AD patients.

In pursuit of this goal, there is a need for more effective and precise methods of analysing amyloid material. In this work, the aim was to improve the read outs of techniques that are currently used, and to develop novel methods for amyloid detection. The main focus has been on small molecules that work as light-switch molecules in presence of amyloids, i.e. they exhibit greatly enhanced fluorescence intensity upon binding to amyloid fibrils. I have characterised the classic amyloid stain thioflavin-T (ThT), and showed how it can differentiate between different amyloid samples based on their morphological attributes, particularly upon detection of its fluorescence lifetime. I have also characterised the binding and fluorescent properties of YOYO-1; a traditional DNA stain that proved to be an attractive alternative to ThT and that therefore may function as a novel amyloid stain, extending the amyloid recognition toolbox.

The Thesis also outlines the development of an existing protocol for expression and purification of monomeric seed-free amyloid- $\beta$ (1-42) that has been setup in our laboratory in order to facilitate reproducible investigation into the formation kinetics of  $A\beta$ (1-42) fibrils.

This work is a stepping stone towards studies of amyloid- $\beta$  formation kinetics and neurotoxicity. I intend to utilise the fluorescence techniques described herein, together with the developed protocol for  $A\beta$  production, to explore different stages of  $A\beta$  aggregation; how they exert their neurotoxic effects, and if these properties are modulated by lipid membranes and molecular crowding effects.

## List of publications

This thesis is based on the following publications, referred to in the text by Roman numerals:

- I. Steady-state and time-resolved Thioflavin-T fluorescence can report on morphological differences in amyloid fibrils formed from A $\beta$ (1-40) and A $\beta$ (1-42).  
David J. Lindberg, Moa S. Wranne, Mélina Gilbert-Gatty, Fredrik Westerlund, and Elin K. Esbjörner  
*Biochemical and Biophysical Research Communications*, **2015**, issue 458, pp. 418-423 (doi: 10.1016/j.bbrc.2015.01.132)
  
- II. Detection of Amyloid- $\beta$  fibrils using the DNA-intercalating dye YOYO-1 – binding mode and fibril formation kinetics  
David J. Lindberg and Elin K. Esbjörner  
*Submitted to Biochemical and Biophysical Research Communications*, **Nov 2015**

## Contribution report

- I. I planned and performed all the experiments together with M.S.W. I analysed the results and contributed to writing the paper.
- II. I conceived the idea, contributed to planning and outlining the work, did all the experiments, analysed the data and wrote the paper together with E.K.E.

## Keywords

Amyloid fibrils, Alzheimer's disease, Amyloid- $\beta$ , Fluorescence spectroscopy, Thioflavin-T, YOYO-1, Linear dichroism

## Abbreviations

A $\beta$	Amyloid- $\beta$ peptide
ThT	Thioflavin-T
AFM	Atomic force microscopy
TCSPC	Time-correlated single photon counting
AD	Alzheimer's disease
APP	Amyloid precursor protein
BACE-1	$\beta$ -site APP-cleaving enzyme 1
CD	Circular dichroism
LD	Linear dichroism
NMR	Nuclear magnetic resonance
CR	Congo red
R6G	Rhodamine-6G
EDTA	Ethylenediaminetetracetic acid
DEAE	Diethylaminoethanol
SDS-PAGE	Sodium dodecylsulphate polyacrylamide gel electrophoresis
YO	Oxazole yellow

# Table of Contents

<b>Introduction</b> .....	1
<i>Alzheimer's disease</i> .....	2
<i>The amyloid-<math>\beta</math> peptide – production and amyloid formation</i> .....	3
<i>Protein folding and misfolding</i> .....	4
<i>Amyloid fibrils and amyloid detection</i> .....	5
<i>Kinetics of amyloid growth</i> .....	7
<i>Amyloid-<math>\beta</math> fibril structure and polymorphism</i> .....	9
<b>Methodology</b> .....	11
<i>Absorption and fluorescence</i> .....	11
<i>Fluorescent molecules and molecular rotors</i> .....	15
<i>Polarized Light Spectroscopy</i> .....	16
<i>Atomic Force Microscopy</i> .....	18
<b>Recombinant expression and purification of monomeric amyloid-<math>\beta</math></b> .....	20
<i>Cloning and expression</i> .....	20
<i>Purification</i> .....	20
<i>Amyloid fibril formation controls</i> .....	22
<b>Study I – ThT fluorescence as a tool to differentiate between amyloid fibrils</b> .....	24
<i>Background</i> .....	24
<i>A<math>\beta</math>(1-40) and A<math>\beta</math>(1-42) produces different ThT emission in concentration-matched samples</i> .....	24
<i>The emission differences are explained by morphological features of A<math>\beta</math> fibrils</i> .....	26
<i>Further investigation into the thioflavin-T fluorescence lifetime</i> .....	27
<b>Study II – YOYO-1 as a novel amyloid fibril fluorescent stain</b> .....	29
<i>Background</i> .....	29
<i>Absorption shift and emission increase of YOYO-1 in presence of A<math>\beta</math>(1-42)</i> .....	30
<i>Comparison of YOYO-1 amyloid fluorescence to YOYO-1 DNA fluorescence</i> .....	31
<i>YOYO-1 as a probe for amyloid formation kinetics</i> .....	32
<b>Summary and Outlook</b> .....	33
<b>Acknowledgments</b> .....	33
<b>References</b> .....	34

## Introduction

*“The first symptom the 51-year old woman showed was the idea that she was jealous of her husband. Soon she developed a rapid loss of memory. She was disoriented in her home, carried things from one place to another and hid them, sometimes she thought somebody was trying to kill her and started to cry loudly. In the institution her behaviour showed all signs of complete helplessness. She is completely disoriented in time and space. Sometimes she says that she does not understand anything and that everything is strange to her. Sometimes she greets the attending physician like company and asks to be excused for not having completed the household chores, sometimes she protests loudly that he intends to cut her, or she rebukes him vehemently with expressions which imply that she suspects him of dishonourable intentions. Then again she is completely delirious, drags around her bedding, calls her husband and daughter and seems to suffer from auditory hallucinations. Often she screamed for many hours.”*

*– Dr. Aloysius ‘Alois’ Alzheimer, Frankfurt, 1901.*

The horror described above details the first documented case of the neurodegenerative disorder that we today know as Alzheimer’s disease (AD), after its German discoverer Alois Alzheimer [1]. A pathophysiological hallmark of this disease is the accumulation of proteinaceous plaques in the brain [2]. In 1984 a short 4 kDa peptide was recovered from brain plaques of AD patients; the amyloid- $\beta$  peptide (A $\beta$ ) [3,4]. It is today well established that aggregation of the A $\beta$  peptide into amyloid fibrils [5-7], along with aggregation of another protein, tau [8], are key events in the pathogenesis of AD. For the last 30 years, intensive effort has been committed into detailing the physico-chemical and biological behaviour of the A $\beta$  peptide, in order to (better) understand the origins of this devastating and increasingly prevalent disease, and to aid in the development of effective treatments. This thesis describes the study of A $\beta$  fibrils, how they form, and how they interact with two fluorescent dyes, thioflavin-T and YOYO-1. Thioflavin-T is a classical amyloid stain; we have characterised its ability to distinguish between amyloid species. YOYO-1 is a DNA stain, which we have characterised for use as an amyloid stain. Better understanding of how amyloid fibrils interact with fluorescent dyes not only enables more efficient use of fluorescence-based techniques for studies of amyloid fibrils, but can also give us structural insight on amyloid fibrils, and how they relate to the aetiology of Alzheimer’s disease.

## **Alzheimer's disease**

In a report from the WHO Global Burden of Disease it was estimated that dementia contributes to 11.2% of years lived with disability in people aged 60 or older. This is more than e.g. stroke (9.5%), musculoskeletal disorders (8.9%), cardiovascular disease (5.0%) and cancer (2.4%) [9]. By far the most prevalent form of dementia is Alzheimer's disease (AD), accounting for at least 50-60% of all cases worldwide. AD is therefore becoming a major healthcare problem; in 2001 approximately 24 million people suffered from AD, and that figure is expected to rise to roughly 80 million by 2040 as a consequence of our (anticipated) increased life expectancies [10]. Not only is AD a strongly debilitating disease that causes tremendous suffering for patients and their care-givers, but it is also a very costly disease in economic terms, that threatens to put an unbearable burden on our current health care systems. As an example, in 2005 it was estimated that 224,000 of the total 461,000 people with cognitive impairment in the UK reside in institutions at an estimated cost of 8.2 billion US dollars, equivalent to 0.6% of the UK GDP [11]. To this is to be added the substantial cost of residential and family care-givers, in the US in 1998 amounting to 18 billion dollars, mostly due to reduced working hours and psychological strain [12]. It hardly needs to be stressed that solving the problem that is Alzheimer's disease is not only a question of human well-being, but also of large societal interest.

AD is at the present day an incurable disease with an invariably fatal outcome. The treatments that do exist offers symptomatic relief, and consists of deploying acetylcholine esterase inhibitors and/or NMDA-receptor antagonists, in order to assist neurotransmission in the degrading brain. Different strategies are employed in the quest for novel disease-modifying treatments, e.g.  $\beta$ - and  $\gamma$ -secretase inhibition [13],  $A\beta$  immunotherapy [14], and fibril formation modulation [15]. There are also epidemiological studies aiming to find parameters that affect the prevalence of AD. Use of cholesterol-modulating drugs [16], anti-inflammatory drugs [17] and antioxidant intake [18], have all indicated a reduced prevalence of AD. When investigated in proper clinical trials these beneficial effects have, however, been hard to verify.

Part of the incurability problem of AD arises from the lack of efficient diagnostic tools. AD diagnosis today is mostly based on behavioural and psychological testing, presence of AD biomarkers, and brain imaging such as computer tomography (CT) or magnetic resonance imaging (MRI), all of which are non-definitive methods. The definitive confirmation of an AD diagnosis is only possible through post-mortem neuropathological examination. This means that any putative effective treatment is also dependent on the development of better diagnostic tools, in order to administer treatment before the disease has progressed too far.

### **The molecular pathology of AD**

AD is characterised by progressive loss of neuronal function leading to memory impairment, cognitive decline and orientational disability [15]. A main pathological characteristic of AD is the emergence of so-called senile plaques, consisting of insoluble deposits of aggregated protein in the medial temporal lobe and cortical areas of the brain [15]. The major

proteinaceous content of the plaques was determined when a short peptide was purified from brain extracts of AD patients in 1984 by Glenner et al [3]. This peptide was named amyloid- $\beta$  ( $A\beta$ ), and in 1991 the *amyloid hypothesis* was formulated [5-7], in which it was postulated that aggregation of  $A\beta$  into fibrillar plaques initiates a series of events that lead to neuronal loss and cognitive decline in AD. AD is also associated with the aggregation of an intracellular protein; the microtubule-associated protein *tau*, which upon hyperphosphorylation forms so-called neurofibrillary tangles – intracellular protein inclusions that are also typically present in post-mortem tissue samples of human AD brains [8]. It is still debated whether  $A\beta$  or tau is the most promising target for a potential treatment, however, the community is relatively unified in concluding that both proteins are of great importance for a full understanding of the pathology of AD. Recent modelling using *in vitro* neuronal networks has, however, provided experimental evidence for that  $A\beta$  pathology precedes and drives the formation of intra-neuronal tau aggregation [19].

### **The amyloid- $\beta$ peptide – production and amyloid formation**

The  $A\beta$  peptide was found to originate from a larger previously unknown membrane protein, which was given the name Amyloid Precursor Protein (APP) [20]. APP is ubiquitously expressed in many tissues, but is abundant in neuronal synapses. Its biological function is not known, though it has been speculated that APP is involved in ion transport [21] and synapse formation [22]. APP can be cleaved proteolytically by several enzymes, including the  $\alpha$ -,  $\beta$ - and  $\gamma$ -secretases. Cleavage of APP by  $\alpha$ -secretase results in a non-amyloidogenic fragment, whereas cleavage by  $\beta$ - and  $\gamma$ -secretases produces the range of amyloidogenic fragments known as  $A\beta$  peptides (fig. 1).  $\beta$ -secretase ( $\beta$ -site APP cleaving enzyme 1, BACE-1) is a transmembrane enzyme that cleaves APP into two parts, producing the 12 kDa fragment C99. This fragment is thereafter cleaved by  $\gamma$ -secretase to produce the actual  $A\beta$  peptide. The cleavage site for  $\gamma$ -secretase is not well defined, and therefore a number of  $A\beta$  isoforms exists, differing in length, commonly from 38-43 residues.  $A\beta$  peptides are typically named by the length of the peptide from N to C-terminus;  $A\beta(1-40)$  is the most commonly produced cleavage product in the human brain, whereas the second most common variant  $A\beta(1-42)$  has been found to be the more abundant isoform present in mature plaques [23,24].

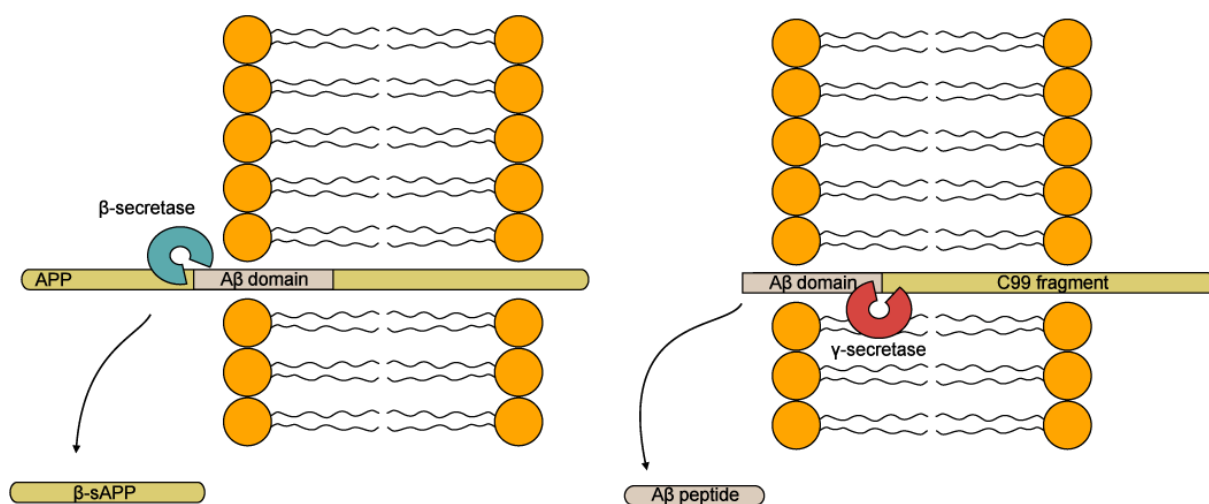


Figure 1. Formation of A $\beta$  peptides by enzymatic cleavage of the amyloid precursor protein (APP) by  $\beta$ - and  $\gamma$ -secretases.

A $\beta$  was originally thought to be an abnormal product related to cellular stress. However it was discovered in 1992 that A $\beta$  is produced continuously under normal metabolic conditions [25], meaning that it exists in both diseased and healthy brains. Recent findings indicate that what causes the accumulation of A $\beta$  is reduced clearance, in contrast to increased A $\beta$  production [26]. It is established that protein homeostasis declines with old age [27], and subsequently, the most significant risk factor for developing AD is increasing age [28].

## Protein folding and misfolding

Proteins are a class of molecules that form a basis for all living matter on this planet. All life forms that are presently identified are sustained by the same basic principle; the genetic code, contained within DNA molecules, is transcribed and translated into proteins that execute the majority of the functions of a living organism. Proteins are polymeric molecules consisting of unbranched chains of amino acids, covalently associated via amide bonds. There are 20 naturally occurring amino acids, which, through a myriad of combinations form the vast range of protein functions that are found in nature. Many of the functions of proteins are dependent on them folding into very precise native structures that make them execute specific cellular functions. Protein folding is a step-wise 'trial and error'-process by which the molecule progressively reaches a thermodynamically more stable conformation [29]. The process is also aided by the presence of chaperones and other molecules that assist proteins in obtaining and maintaining their correct fold, in order to preserve their cellular function. Nevertheless, there are instances when proteins fail to fold properly or fail to maintain their correct fold. This phenomenon, generally referred to as *protein misfolding*, results in several severe and often incurable human diseases that are characterised by accumulation of aggregated protein deposits (see Table 1).

Table 1. Human diseases associated with build-up of amyloid protein deposits (adapted from [30]).

<b>Disease</b>	<b>Associated protein/peptide</b>
<i>Neurological amyloid deposit disorders</i>	
Alzheimer's disease	Amyloid- $\beta$ peptide (A $\beta$ ), Tau
Parkinson's disease	$\alpha$ -synuclein ( $\alpha$ S)
Frontotemporal dementia with Lewy bodies (FTLD)	Tau
Huntington's disease	Huntingtin with poly-Q expansions
Spongiform encephalopathy (Creutzfeldt-Jakob disease)	Prion proteins
Amyotrophic lateral sclerosis (ALS)	Superoxide dismutase 1 (SOD1), TDP-43
<i>Non-neurological systemic disorders</i>	
AL amyloidosis	Immunoglobulin light chain
AA amyloidosis	Serum amyloid A protein
Haemodialysis-related amyloidosis	$\beta$ 2-microglobulin
Familial amyloidotic polyneuropathy	Transthyretin
Lysozyme amyloidosis	Lysozyme
<i>Non-neurological localized disorders</i>	
Type II diabetes	Islet amyloid polypeptide (IAPP)
Injection-localized amyloidosis	Insulin

## Amyloid fibrils and amyloid detection

Upon misfolding, all of the proteins in Table 1 adopt astonishingly similar  $\beta$ -sheet-rich polymeric structures. These were first discovered in 1854, when the German physician Rudolph Virchow poured iodine on a brain sample that had an "abnormal macroscopic appearance" [31]. The iodine stained the sample deep purple, and Virchow thereby concluded that the sample must consist of starch or cellulose (the distinction between the two was unclear in the 19<sup>th</sup> century), naming the newly discovered substance *amyloid* (*Greek*, amylo- – starch). It later turned out that what Virchow discovered was neither cellulose nor starch, but misfolded proteins that had aggregated into what we now call amyloid fibrils. There is growing evidence that the ability to form amyloid fibrils is common to all polypeptide chains [30,32]; indeed it has even been found that peptides consisting of just a couple of amino acids can assemble into fibrils [33]. This generality is likely due to that amyloid fibrils are primarily stabilized by hydrogen bonding interactions involving the peptide backbone, and thus of a chemical structure that is invariant of the amino acid sequence [34]. Despite this, the tendency of a protein to actually form amyloid fibrils correlates strongly with its primary sequence, with high hydrophobic side chain-content and/or inherently disordered structures commonly resulting in a stronger tendency towards amyloid formation [35,36]. Even though naturally occurring amyloid forming proteins differ greatly in primary sequence, the formed fibrils do share a surprising amount of biophysical and structural properties.

## Amyloid fibril structure

Atomic resolution structural information of amyloid fibrils is hard to obtain due to the size, insolubility, and heterogeneity of amyloid assemblies, which complicates the use of traditional structural biology methods such as NMR spectroscopy and X-ray crystallography. Instead combinatorial approaches involving several time-consuming experimental methods are often required to achieve high-resolution structures [37]. Amyloid fibrils exhibit a characteristic diffraction pattern when placed in an X-ray beam, reminiscent of a cross [38], which gives rise to the name of the structural feature that makes up the core of the amyloid fibril; a *cross- $\beta$*  fold. It consists of two or more  $\beta$ -strands that form a highly stable antiparallel or parallel  $\beta$ -sheet motif (fig. 2). Therefore, secondary structure determination methods such as circular dichroism spectroscopy reveal that amyloid fibrils are strongly dominated by  $\beta$ -sheets, and it has been shown by linear dichroism spectroscopy [39] and polarized fluorescence microscopy [40] that the  $\beta$ -sheets of the cross- $\beta$  core are aligned perpendicularly to the long axis of the fibril. Quaternary association of these  $\beta$ -sheet-rich monomers through stacking leads to the formation of long extended fibrillar assemblies. The two reflections in the diffraction pattern are located at approximately 10 Å and 4.7 Å, corresponding to two characteristic spacings between  $\beta$ -sheets in the amyloid fibril (fig. 2); The 10 Å reflection corresponds to the interstrand spacing; the distance between the two  $\beta$ -sheets that make up each individual monomer. The second is the stacking distance between each set of monomers. These structural commonalities provide amyloid fibrils with certain common biophysical characteristics, despite major differences in the primary sequence of the monomer.

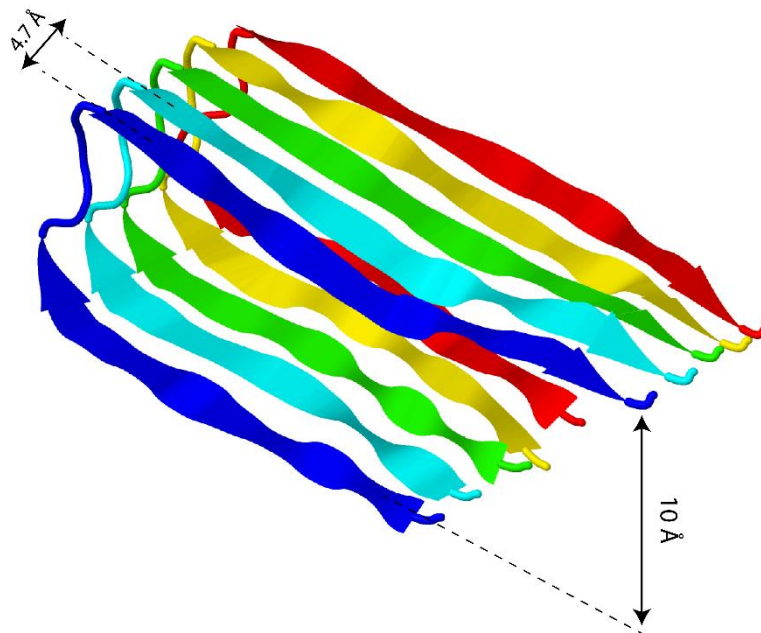


Figure 2. Three-dimensional representation of the secondary and tertiary structure of an amyloid fibril. This example shows 5 monomers of an  $A\beta(1-40)$  fragment that are associated by hydrogen bonding into a protofilament of an amyloid fibril. The drawing shows the two distinctive spacings that are present in the cross- $\beta$  core of all amyloid fibrils; the 10 Å spacing is the distance between the two sheets in the  $\beta$ -hairpin of each individual monomer, whereas the 4.7 Å spacing is the distance between two neighbouring monomers in the fibril stack. Image retrieved from the Protein Data Bank, published in Luhrs et. al [41] PDBID: 2BEG.

## Amyloid fibril detection

As a consequence of the structural similarity between different amyloid fibrils, it is possible to detect them using various general amyloid-binding molecules. Traditionally, the hallmark of amyloid detection has been the observation of apple-green birefringence upon staining with Congo red (CR) [42]. A more straightforward, and today more common method is the use of thioflavin-T (ThT) fluorescence. ThT is a dye that is nearly non-fluorescent in water, but exhibits up to a 1000-fold increase in quantum yield upon binding to different amyloid fibrils [43]. Both CR and ThT were established as amyloid stains well before their general structural features were established; therefore the mechanisms of binding are not fully characterised. With atomic-level structure determination being very time-consuming, fluorescence-based techniques are essential in studies of amyloid fibrils, as they provide a quick and reliable way of evaluating the presence and state of amyloid fibrils. Fluorescence is especially useful in experiments dealing with the kinetics of amyloid fibril formation, as emission from amyloid-binding dyes has proven to be a very successful technique for reproducible measurement of the formation of amyloid fibrils.

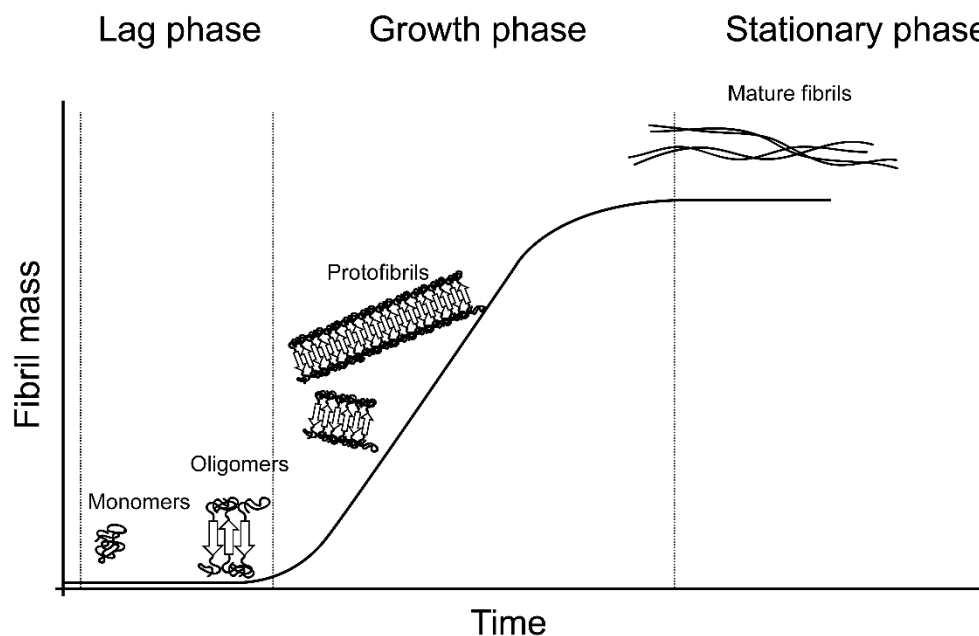


Figure 3. Schematic illustration of the kinetics of amyloid fibril growth. Early on in the lag phase, the reaction is dominated by nucleation events and the fibril mass grows very slowly. As more and more oligomeric seeds are formed, fibrils start growing, and secondary nucleation processes occur, thereby dramatically increasing the fibril growth rate. When the monomer is depleted the reaction has reached a stationary phase, where most of the material is gathered in mature amyloid fibrils that are typically laterally associated to each other.

## Kinetics of amyloid growth

The abundance of mature amyloid plaques in AD brains does not correlate with neuronal loss [44]. Instead, attention has shifted towards different small oligomeric amyloid species that are only transiently formed during the amyloid formation reaction [45,46]. This highlights the

need for a detailed understanding of how and why amyloid fibrils form in real-time. The principles governing the kinetics of amyloid- $\beta$  aggregation *in vitro* are becoming increasingly well understood. Amyloid formation is a nucleation dependent polymerisation process that is initiated by a primary nucleation step. However, the progression of amyloid formation has been shown to involve different modes of secondary nucleation (i.e. nucleation events involving already formed fibrils) and fragmentation, resulting in the appearance of sigmoidal growth kinetics when the change in fibril mass is plotted against time (fig. 3). There are several mathematical models that describe the microscopic series of events underlying the rates of formation of amyloid fibrils [47-50]. In a very elaborate theory of amyloid fibril growth, Knowles et. al [48], divides the growth modes of amyloid fibrils into three separate categories; nucleation and fragmentation events, growth processes, and dissociation processes (fig. 4). Nucleation and fragmentation events lead to the formation of new aggregates. Primary nucleation (formation of oligomers from monomers) results in elongation-competent seeds that initiate fibril growth reactions; these events typically dominate the distinct lag phase that is seen in all amyloid formation reactions where the starting material is monomeric and free of pre-formed seeds (fig 3). Primary nucleation on its own is, however, not enough to explain the rapid growth of amyloid fibrils that occurs once a critical mass of nuclei have formed. In order to explain this kinetic behaviour, fragmentation and secondary nucleation are introduced as further processes by which more nuclei are formed [51]. Fragmentation occurs when a formed fibril is cleaved into two or more shorter pieces, and acts to enhance amyloid formation rates by exponentially increasing the number of free ends in the sample. This phenomenon can be observed by vigorously shaking a solution of amyloidogenic protein, causing mechanic breaking of existing fibrils, whereupon an increase in the fibril formation rate is observed [52]. Secondary nucleation is a process by which already formed fibrils catalyse the formation of new oligomers, probably by means of surface interactions. The great importance of secondary nucleation has only been discovered recently, and as such, the exact mechanisms of how this catalysis occurs are yet not known [51].

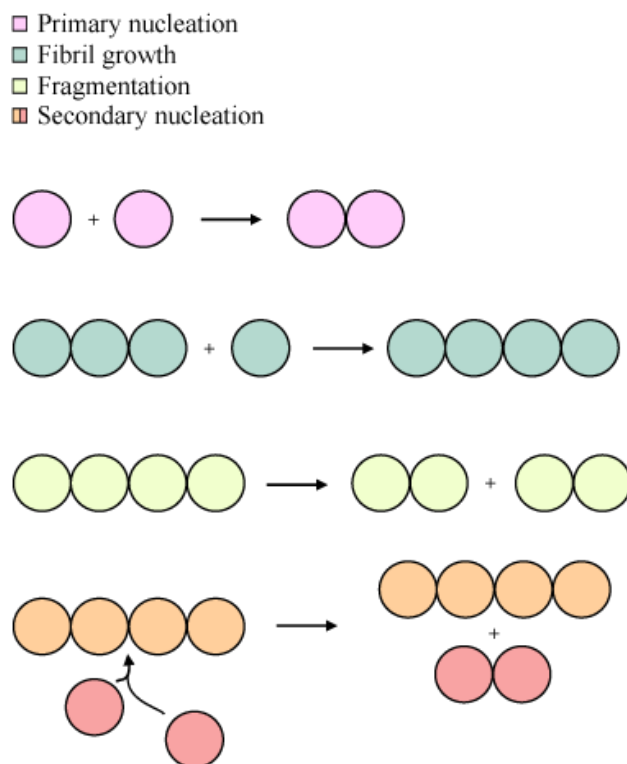


Figure 4. Scheme detailing the different processes contributing to the growth of amyloid fibrils.

Growth processes elongate fibrils by addition of monomers to the ends of the growing fibril. Kinetic studies have revealed that this process has a first-order concentration dependence on both fibril and monomer concentration. This highlights that the growth of amyloid fibrils occurs through monomer addition only, and not oligomer addition, which would cause a non-linear dependence on the monomer concentration [53]. At high concentrations, the structural reorganisation upon monomer addition becomes rate-limiting, and the overall growth rate becomes zero-order dependent on the monomer concentration. Dissociation processes are typically much slower than growth processes in amyloid formation, and as such, they only play a major role once the monomer pool is nearly depleted by the end of the reaction [54].

### Amyloid- $\beta$ fibril structure and polymorphism

The two most common isoforms of A $\beta$ , the 40-residue and 42-residue length peptides, have been extensively studied in order to reveal both their monomeric and their fibrillar molecular structures. Still, it is not clear why the 42-residue peptide is more neurotoxic to nerve cells than its 40-residue counterpart. One reason for this is that consensus structures have been difficult to assemble due to both peptides exhibiting considerable structural polymorphism in their amyloid states. Different A $\beta$  preparation methods and different synthesis methods can lead to very different structures [55]. This is generally thought to be an effect that also occurs *in vivo*, which further complicates the search for a distinct disease-causing species of A $\beta$  fibrils. On a general level, all fibrillar species and most small species are predominantly composed of  $\beta$ -sheets. A mature fibril consists of one or several protofilaments. Most models describe a two-

fold symmetry between protofilaments, where the fibril core consists of two filaments laterally associated to each other. There are, however, other models suggesting e.g. a three-fold symmetry with three filaments associating in a triangular shape to make up the fibril core [56,57].

# Methodology

## Absorption and fluorescence

One early observation of the physical process we now know as fluorescence was when Sir John Fredrich William Herschel in 1846 let sunlight shine on a solution of quinine, and observed a “beautiful celestial blue colour”. While Herschel could not explain this spectacular phenomenon in the mid-19<sup>th</sup> century, we now have an extensive understanding of fluorescence [58]. To understand fluorescence, we need first to consider the absorption of light by molecules.

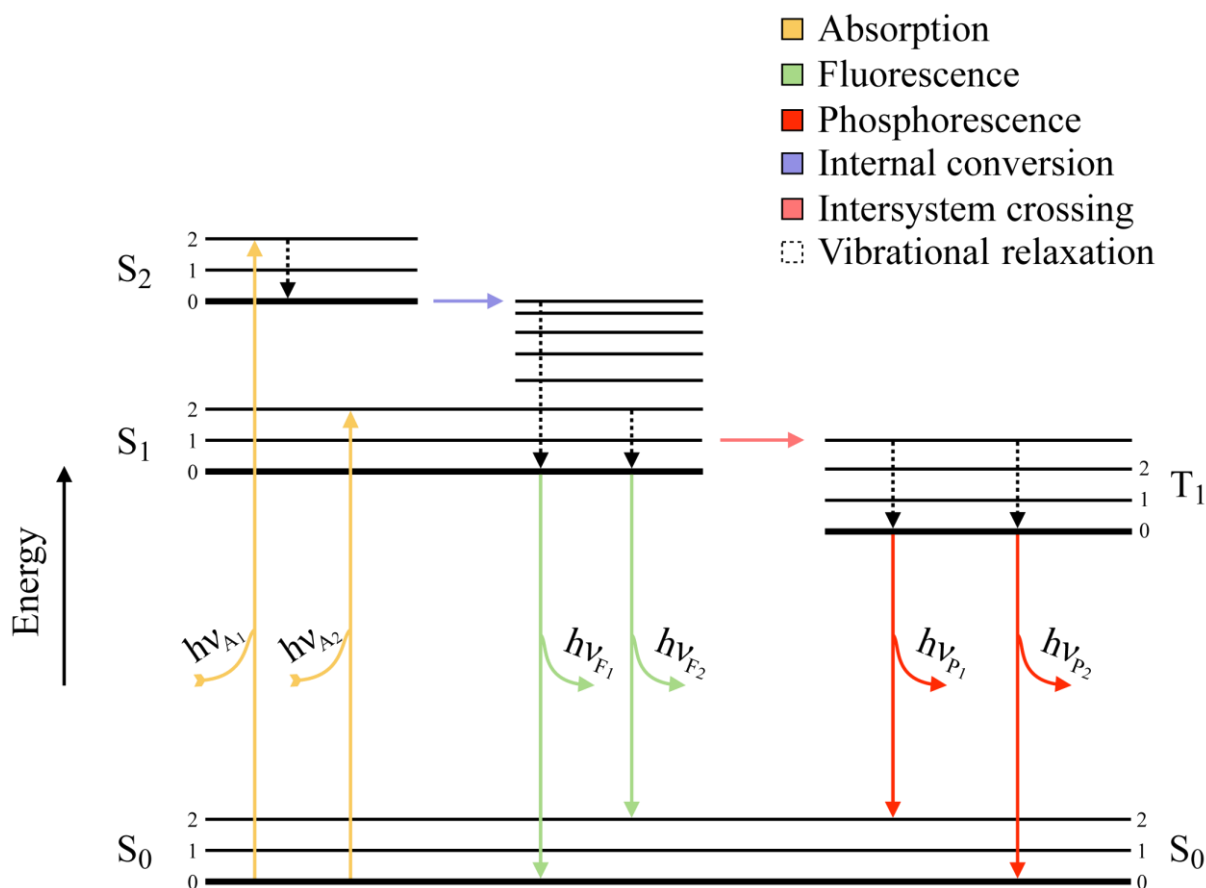


Figure 5. Jablonski energy diagram describing the physical processes involved in absorption, fluorescence and phosphorescence.

Any atom or molecule can be described in terms of an energy diagram (fig. 5). The energy diagram contains a representation of the different energetic states in which the molecule can exist, where the lowest energy state is called the ground state (S<sub>0</sub>), and any state higher in energy is called an excited state (S<sub>1</sub>, S<sub>2</sub>, etc.). If the molecule interacts with a photon that energetically matches an energy gap between two states, the molecule has a probability of absorbing the energy of the photon, thereby transitioning into the higher state. This is called the Bohr frequency condition, and is a direct consequence of the Planck-Einstein relation (eq. 1) which relates photon energy (E) to its frequency ( $\nu$ ) or wavelength ( $\lambda$ ), and where  $h$  is Planck’s constant, and  $c$  is the speed of light.

$$E = h\nu = \frac{hc}{\lambda} \quad (1)$$

This process by which photon energy is transferred to molecules is called absorption, or in the context of fluorescence, excitation. A molecule which has absorbed energy and transitioned into a higher energetic state is called an excited molecule. As nature strives for energy minimisation, an excited state is usually relaxed back down to the ground state very rapidly. This can occur through a number of different processes, the ones most relevant to this work are listed in figure 5.

Fluorescence is the process when relaxation occurs through the release of a photon. The emitted photon is usually lower in energy than the absorbed photon. This is called the Stokes' shift, and happens because the molecule rearranges itself internally before the emission event happens; therefore some of the some excitation energy is released as heat, and the emitted photon has lower energy than the absorbed photon. Sometimes a molecule transitions into what is called a triplet state through a process known as intersystem crossing. Relaxation from the triplet state is a forbidden transition, and therefore, emission from this state is very long-lived, and goes by a specific name, phosphorescence.

### **Absorption and fluorescence spectroscopy**

In absorption spectroscopy, a sample can typically be irradiated with light of a fixed frequency. The intensity of light that passes through the sample ( $I$ ) is then detected and compared to the initial light intensity ( $I_0$ ) (eq. 2), in order to determine the amount of light that was absorbed by the sample. The logarithm of this value is the absorptivity ( $A$ ).

$$A = \log \frac{I}{I_0} \quad (2)$$

Measuring the absorptivity over a range of wavelengths gives an absorbance spectrum, which is the absorptivity of the sample, plotted against the wavelength of absorbed light. Figure 6 shows the absorbance spectrum of rhodamine-6G (R6G), a commonly used fluorescent dye. The absorbance spectrum shows that R6G absorbs visible light in a wavelength region between ~450 nm and 575 nm, with the absorbance maximum being 530 nm.

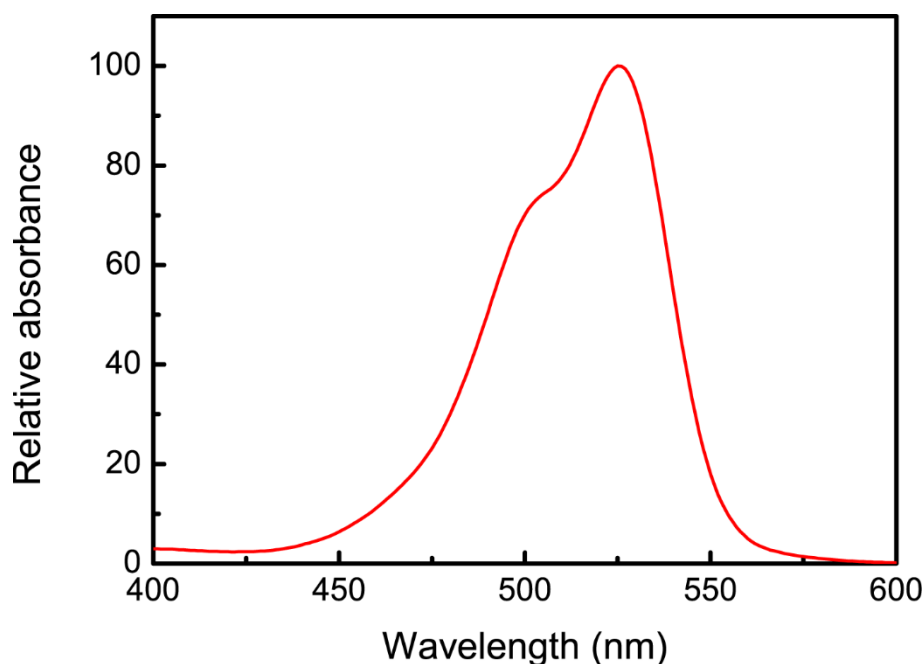


Figure 6. Absorption spectrum of rhodamine-6G in water. Data retrieved from <https://www.thermofisher.com/se/en/home/life-science/cell-analysis/labeling-chemistry/fluorescence-spectraviewer.html>

Steady-state fluorescence spectroscopy is similar to absorption spectroscopy. The sample is irradiated by a wavelength of light that is absorbed by the molecule of interest, typically at or near the absorption maximum, to achieve maximum efficiency. Instead of detecting the amount of light that is absorbed by the sample, one measures the amount of photons that are emitted through fluorescence. This is done by exciting the sample with light of a fixed wavelength, and then measuring the amount of photons emitted at another wavelength. The plot of emission intensity versus the wavelength of emission is called an emission spectrum, and describes the relative intensity of fluorescence emission of a molecule. Continuing with the example of R6G, we observe that this molecule emits light in a range between 500 and 700 nm, with an intensity peak at 566 nm (fig 7, red curve). Similarly, one can record the excitation spectrum; emitted photons are then detected at a fixed wavelength, and different excitation wavelengths are scanned to produce a record of the excitation intensity. An excitation spectrum thereby describes the absorption spectrum of only the emitting species. In the case of R6G, we find that the optimal excitation is 530 nm, which is the same wavelength as the absorption maximum.

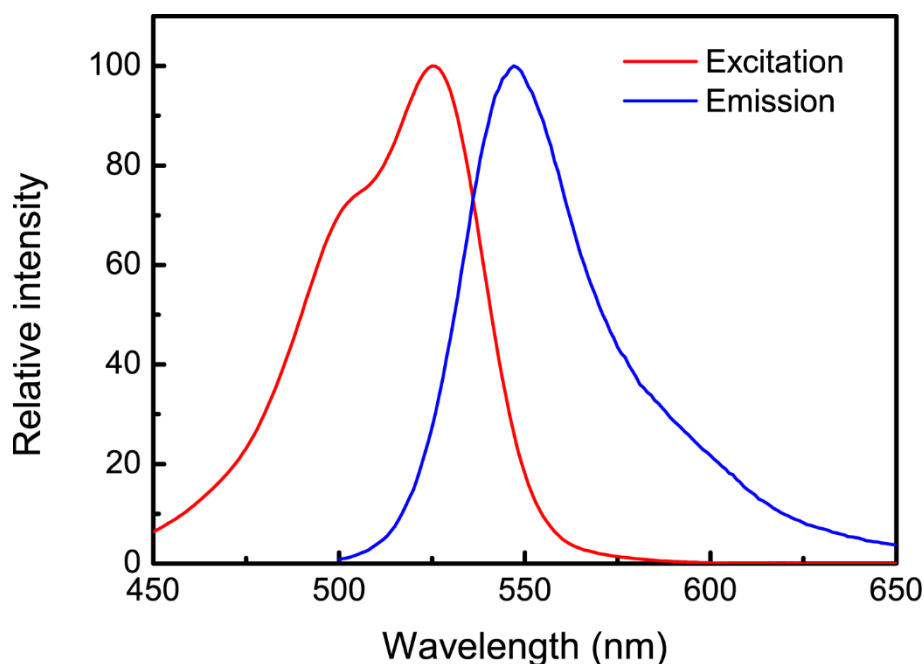


Figure 7. Excitation (red) and emission (blue) spectra of Rhodamine-6G in water. The Stoke's shift is given by the separation of the two peaks. Data retrieved from <https://www.thermofisher.com/se/en/home/life-science/cell-analysis/labeling-chemistry/fluorescence-spectraviewer.html>

In many experimental techniques where fluorescence is used as a means of detection, one is mainly concerned with the intensity of fluorescence emission and not with the time-scales on which the emission processes occur. However, it can prove useful to measure the time-dependence of fluorescence emission by *time-resolved fluorescence spectroscopy*, a method that detects the time that passes between the excitation event and the emission event. This time, which is called the lifetime of fluorescence ( $\tau$ ), is an intensive property that is specific for any given fluorophore in a given set of conditions, and it is typically affected by e.g. the chemical environment of the fluorophore. Fluorescence emission is a random event, meaning that for an ensemble of excited molecules, the time spent in the excited state will be a distribution of times corresponding to an exponential decay function (eq. 3), which describes the time-dependent decay of the emission intensity. If the intensity decay function is multi-exponential ( $i > 1$ ), the fluorophore has several distinct fluorescence lifetimes.

$$I(t) = \sum_{i=1}^n \alpha_i e^{-t/\tau_i} \quad (3)$$

One method of determining the fluorescence lifetime is by time-correlated single photon counting (TCSPC). In principle, the time between excitation and emission is measured for a high number of emission events using a high-frequency pulsed light source (typically a laser). These times are then collected into a histogram describing the time-resolved decay of the molecule's excited state. Using non-linear regression, this decay can be fitted to a multi-exponential function (eq. 3) and we can extract the fluorescence lifetime(s) ( $\tau$ ) of the molecule. The lifetime of the excited state typically changes depending on factors such as the physico-chemical environment of the fluorophore. It is therefore possible to draw conclusions about

e.g. different binding sites by measuring the time-resolved fluorescence of a bound dye. An inherent advantage of fluorescence lifetimes is that they are concentration-independent, whereas the steady-state emission intensity is dependent on e.g. the concentration of the fluorescent molecule.

## Fluorescent molecules and molecular rotors

Molecules that relax their excited state energy through fluorescence emission are called fluorophores. Proteins themselves often contain or are associated with intrinsic fluorophores, such as the amino acids tryptophan and tyrosine or the protein cofactor NADH. However, most fluorophores used in biological experiments are not intrinsic, but extrinsic, meaning that they are not a natural part of the system one wants to investigate. Instead they are associated to a protein of interest, either by non-covalent interactions, by covalent chemical conjugation, or by cloning and recombinant expression of fusion proteins carrying a fluorescent protein such as GFP (green fluorescent protein) [59]. A specific class of fluorophores that is of special interest in the context of amyloid fibril research are the so-called *molecular rotors*; they are molecules with fluorescence properties that are strongly dependent on their abilities to rotate around a chemical bond(s). A molecular rotor is typically nearly non-fluorescent in water solutions, where the rotational relaxation of its excited state is very fast. However, in a restricted environment where the rotational motion is hindered or reduced, e.g. in a viscous solution or bound to a substrate, its emission intensity is increased by several orders of magnitude, producing a 'light-switch' effect. The work in this Thesis concerns two molecular rotors; thioflavin-T and YOYO-1.

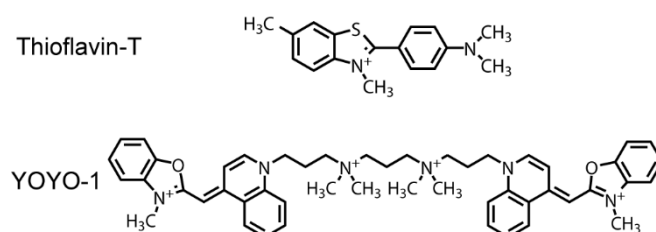


Figure 8. Chemical structure of, Top: the amyloid binding dye thioflavin-T (ThT). Bottom: the DNA intercalator YOYO-1.

### Thioflavin-T

Thioflavin-T (ThT) is a benzothiazole dye (fig. 8) that, although it has been known to stain amyloid structures since the 1950's, saw a widespread increase in usage in the early 1990s as the amyloid origins of Alzheimer's disease pathology was proposed. ThT is a molecular rotor; upon binding to amyloid fibrils, rotation around the central carbon-carbon bond is restricted, and the emission from ThT is increased by up to three orders of magnitude [60]. ThT stains almost all kinds of amyloid fibrils, (some repetitive polypeptides excluded, e.g. polyglutamate fibrils that occur in Huntington's disease) suggesting that it must bind to a common structural element. Studies using polarized fluorescence microscopy and linear dichroism have provided convincing evidence that ThT binds in groove-like channels that are formed by amino acid

side-chains protruding from the  $\beta$ -sheets that make up the fibrillar cross- $\beta$  core [39,40,61]. This is further demonstrated by the structural similarity of many amyloid-binding molecules, such as thioflavin-T, congo red, chrysamine-G, PTAA, Pittsburgh compound B, and other amyloid-binding molecules that are all small aromatic molecules with elongated shapes [62]. This type of channel-binding is reminiscent of groove-binding in double-stranded DNA, and curiously enough, there are also studies showing the binding of ThT to double-stranded DNA [63].

### **YOYO-1**

YOYO-1 is a homodimeric molecule consisting of two monomers of oxazole yellow (YO) bound together by an amine linker (fig. 8). It is a molecular rotor, like ThT, and as such, it is nearly non-fluorescent in aqueous solution [64]. Traditionally, YOYO-1 is used as a fluorescent DNA stain. It binds to double-stranded DNA and intercalates its two chromophores between the base-pairs in the DNA stack, leading to restriction of the rotational freedom in the YO moieties, and to a dramatic increase in emission [65]. YOYO-1 is widely used due to its low background fluorescence, its high extinction coefficient ( $98,000 \text{ M}^{-1}\text{cm}^{-1}$ ), and its strong binding affinity for double-stranded DNA. It belongs to a family of homodimeric cyanine DNA-binding dyes, all together covering a large portion of the visible spectrum. The elongated shape and the molecular rotor nature, together with the favourable spectral properties of YOYO-1, sparked our interest into investigating the use of YOYO-1 to study amyloid fibrils.

### **Polarized Light Spectroscopy**

Polarized light spectroscopy is a kind of differential absorption spectroscopy where the difference in absorption between light of different polarisation is measured. Two kinds of polarised light spectroscopy have been used in this work: circular dichroism (CD), and linear dichroism (LD). CD is the difference in absorbance of right-handed vs. left-handed polarised light in a sample. CD will give information on the presence of chiral centres in the molecule, and is a technique that has become particularly useful to study proteins or DNA, both of which contain chiral carbon atoms in their backbone structures. In proteins, the chiral carbon atoms that make up their peptide backbone give rise to CD spectral shapes that are characteristic to different secondary structure elements of proteins ( $\alpha$ -helices,  $\beta$ -sheets, etc.), making CD the primary tool to estimate protein secondary structure. In the context of amyloid fibrils, CD can be used to monitor the  $\beta$ -sheet content of a sample, thereby directly assessing the fibril formation as the protein transitions from a statistical coil to a  $\beta$ -sheet rich structure. Figure 9 shows the change in CD as a solution of A $\beta$  aggregates into amyloid fibrils. Initially, the protein is in a statistical coil structure, as indicated by a negative peak at 200 nm (dark colours). As the protein aggregates into amyloid fibrils (light colours), the negative peak is shifted towards 218 nm, representing formation of  $\beta$ -sheet structures in the sample.

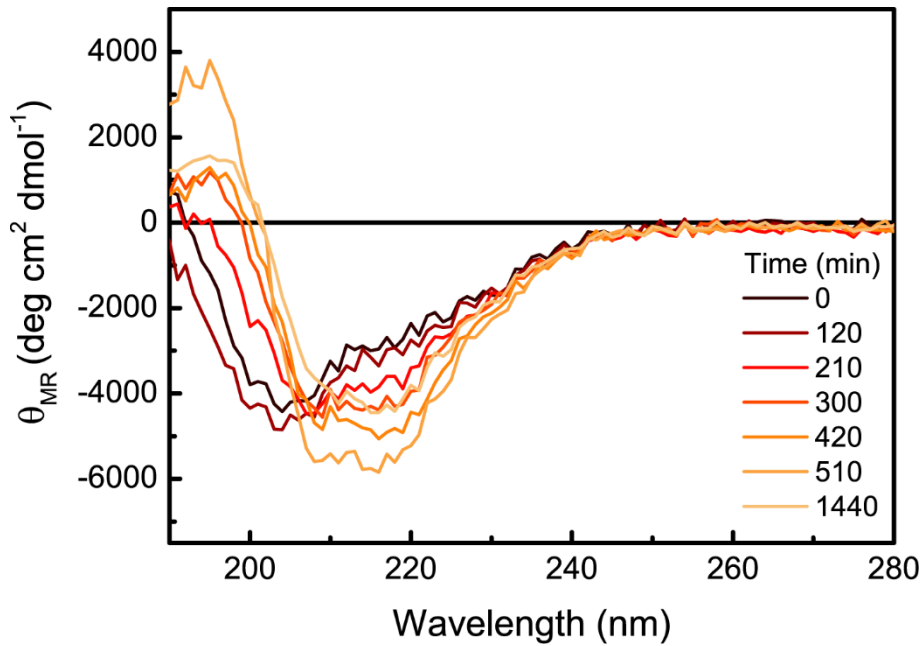
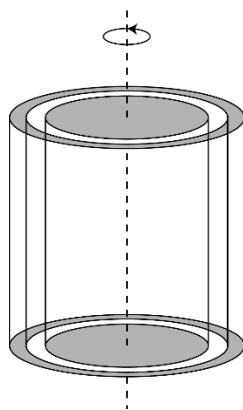


Figure 9. Formation of amyloid fibrils by A $\beta$ (1-42) followed by circular dichroism. The formation of  $\beta$ -sheets associated with amyloid fibril formation is observed as a relative increase in the negative peak at 218 nm compared to the negative peak at 200 nm.

Linear dichroism is a technique similar to CD, but based on linearly polarised light instead of circularly polarised light. The probability of absorption is dependent on the angle between the electric component of the photon, and the electric dipole moment of the molecule. This means that the orientation of a molecule will determine the likelihood of absorption to occur when a molecule is irradiated with linearly polarised light. In an LD measurement, the sample is irradiated with light polarised parallel and perpendicular to an orientation axis, and the difference between these two irradiation modes is measured (eq. 4).

$$LD = A_{\parallel} - A_{\perp} \quad (4)$$

A randomly oriented population of molecules will absorb both these two polarisations to the same extent, and the linear dichroism is therefore zero. However, if a sample is in some way aligned so that the dipole moments of the absorbing molecules are oriented in relation to the orientation axis, the difference in absorption of the two polarisations will be non-zero, thereby giving rise to a linear dichroism spectrum.



*Figure 10. A couette flow cell, with two concentric glass cylinders. In the experimental setup used in this work, the outer cylinder is rotating around the dashed rotational axis, and the inner cylinder is fixed. This creates a hydrodynamic shear flow between the two cylinders.*

In the case of protein polymers, such as amyloid fibrils, one can orient a sample by introducing it into a hydrodynamic shear flow. The fibrils will be stretched out in the direction of the flow, and thereby be oriented in relation to the orientation axis of the instrument. In this work, this is done using a glass Couette flow cell; a rotating glass tube with a fixed glass cylinder on the inside (fig. 10). If a solution is introduced between the cylinder and the tube, the solution will form a hydrodynamic flow, and molecules above a certain size (related to the shear rate of the flow) will become oriented along the radial axis of the flow cell. LD thereby selectively measures absorption properties of only oriented molecules, and can therefore be effectively used to study binding of small molecules to biopolymers. A typical fluorophore is too small to orient in a hydrodynamic flow, but upon binding to an amyloid fibril, it acquires the orientation of the amyloid fibril, and therefore produces an LD signal.

## **Atomic Force Microscopy**

Atomic force microscopy (AFM) is a scanning-probe microscopy technique that is especially sensitive in scanning height differences in the z-direction, making it very well suited for studies of e.g. surface structures or molecules immobilized on surfaces. In AFM, a very small scanning tip (probe) is attached to the bottom of a flexible cantilever. The cantilever is then positioned above the sample and the tip is moved towards the surface. When the tip approaches an object, van der Waal's forces will cause the cantilever to deflect. This deflection can then be very precisely detected by aiming a laser at the cantilever and measuring how the laser light reflection changes (fig. 11), thereby measuring how the tip reacts to objects directly beneath it. Usually a feedback mechanism is employed to ensure that the tip does not make actual contact with the surface, but rather hovers above the surface at a constant force, and the signal is instead determined by monitoring feedback voltage. This technique is called semi-contact AFM, as the probe is not in contact with the surface. The lateral resolution of AFM is governed by the size of the probe and the precision of the piezo-electric systems that control the scanning, both of which can be manufactured to achieve sub-nanometre resolution, several orders of magnitude higher than that of a conventional optical microscope.

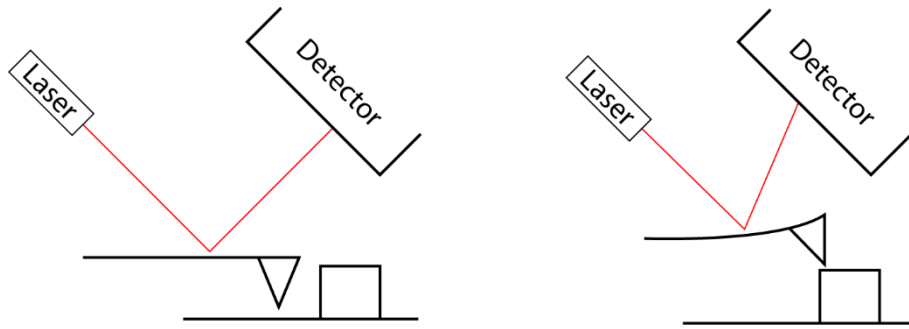


*Figure 11. Schematic figure of an AFM microscope illustrating how the cantilever holding the tip is deflected upon interaction with the substrate, thereby causing a reflection of the laser beam.*

## Recombinant expression and purification of monomeric amyloid- $\beta$

Accurate accounts on the kinetics of amyloid fibril formation can only be obtained with careful control of the nature of the starting material. It is therefore necessary to obtain highly monomeric solutions as starting material so that the rates of formation under seed free conditions may be established. For this purpose, this Thesis describes the adaptation and further development of a protocol for expression and purification of highly monomeric seed-free amyloid- $\beta$ (1-42). The protocol builds on the method originally described by Walsh and Linse [66]. As A $\beta$ (1-42) is sequestered to inclusion bodies in *E. coli* [66], the purification procedure therefore requires purification of inclusion bodies followed by solubilisation in order to release the expressed protein.

### Cloning and expression

Sequence-verified PetSac plasmids containing the A $\beta$ (1-40) and A $\beta$ (1-42) genes (gift from Prof. Sara Linse at Lund University) were transformed into an expression strain of *E. coli* (BL21 DE3) by calcium-heat shock and spread on ampicillin (50 mg/ml) LB agar plates. Single colonies were picked and inoculated into ampicillin LB (50 mg/ml) and kept as frozen glycerol stocks at -80°C. Plasmids were also transfected analogously into *E. coli* (DH5 $\alpha$ ) for future plasmid preparation and potential cloning experiments.

For expression of A $\beta$ (1-42), a PetSac plasmid carrying a synthetic gene of the human A $\beta$ (1-42) peptide (gift from Prof. Sara Linse, Lund University) was inserted into *E. coli* (strain BL21 (DE3) pLysS) and grown on LB agar plates (10 g L<sup>-1</sup> tryptone, 5 g L<sup>-1</sup> yeast extract, 10 g L<sup>-1</sup> NaCl, 15 g L<sup>-1</sup> agar) containing ampicillin (50  $\mu$ g/ml) and chloramphenicol (34  $\mu$ g/ml) overnight. A single colony was picked and inoculated into an overnight culture of 10 mL LB medium (10 g L<sup>-1</sup> tryptone, 5 g L<sup>-1</sup> yeast extract, 10 g L<sup>-1</sup> NaCl) containing ampicillin (50  $\mu$ g/ml) and chloramphenicol (34  $\mu$ g/ml). The following day, 750 mL of ZYM-5052 auto-inducing cell culture medium (1% tryptone, 1% yeast extract, 25 mM Na<sub>2</sub>HPO<sub>4</sub>, 25 mM KH<sub>2</sub>PO<sub>4</sub>, 50 mM NH<sub>4</sub>Cl, 5 mM Na<sub>2</sub>SO<sub>4</sub>, 2 mM MgSO<sub>4</sub>, 0.2X trace metal solution, 0.5% glycerol, 0.05% glucose and 0.2% lactose) [67] was inoculated with the pre-culture and incubated at 37° C, 180 rpm shaking overnight to induce protein expression. The cells were harvested the morning after by centrifugation at 4,500x g for 20 min. The cell pellet was reconstituted in 100 mM Tris-HCl, 10 mM EDTA, pH 8.0 and frozen at -20° C until further use.

### Purification

To purify A $\beta$ -containing inclusion bodies, a frozen *E. coli* pellet was thawed in lukewarm water and then sonicated for 3 minutes (2 seconds on, 2 seconds pause) at 70% amplitude using a Vibra-cell tip-sonicator (Sonics). The sonicated cells were centrifuged at 22,000x g, 4° C for 10 minutes to pellet cellular material. The pellet was reconstituted in buffer, discarding the

supernatant, and the sonication-centrifugation cycle was repeated. After the final sonication-centrifugation cycle, the pellet was transferred to a homogeniser for solubilisation

The purified inclusion bodies were solubilized in 20 mL 8 M urea, 10 mM Tris-HCl, 1 mM EDTA, pH 8.0 and thereafter diluted to 2 M urea with buffer. The solution was mixed with approximately 5 grams of DEAE anion exchanger (Whatman) and stirred for 30 minutes at 4° C. The slurry was filtered onto a filter paper in a Buchner funnel, and then washed with 20 mL 10 mM Tris-HCl, 1 mM EDTA, pH 8.0, followed by 20 mL 25 mM NaCl in the same buffer. A $\beta$ (1-42) was then eluted with 35 mL 125 mM NaCl. The eluted protein was filtered through a 30 kDa MWCO centrifugal filter to remove large proteins and cellular material, and the protein solution was snap-frozen in liquid nitrogen, freeze-dried in low-binding microcentrifuge tubes (Axygen), and kept at -80° C until further use.

Samples from all steps of the purification procedure were analysed on an SDS-PAGE gel (4-12% Bis-Tris, Invitrogen) to evaluate A $\beta$  purity and expression level, see (fig. 12). A $\beta$ (1-42) is 4.5 kDa in size, and appears as a single band in fig. 5, just above the 3.5 kDa band in the protein ladder.

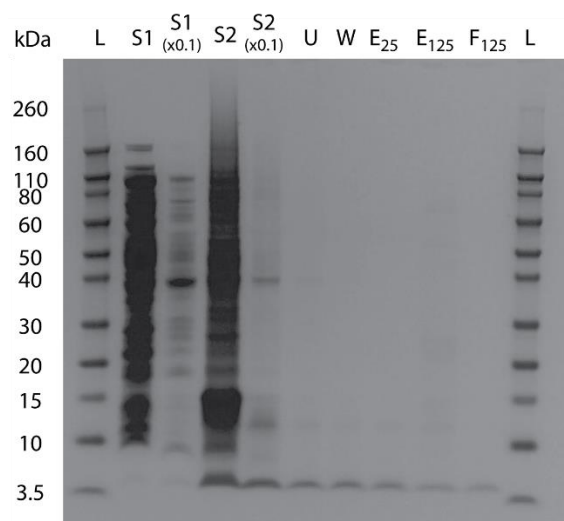


Figure 12. SDS-PAGE of samples recovered during A $\beta$ (1-42) work-up. From left to right: (L): Novex Sharp Prestained Protein Standard, (S1): First sonication supernatant, as is, and 10x diluted, (S2): Second sonication supernatant, as is, and 10x diluted, (U): Flowthrough from urea solubilisation, (W): 10 mM Tris-buffer wash, (E<sub>25</sub>): 25 mM NaCl wash, (E<sub>125</sub>): 125 mM NaCl elution, (F<sub>125</sub>): 30K MWCO-filtered 125 mM NaCl elution. A ~4.5 kDa band corresponding to A $\beta$ (1-42) is visible in all lanes except S1.

Prior to each experiment, a small amount of lyophilized A $\beta$  was reconstituted in 7 M guanidium hydrochloride and incubated on ice for 30 min. The solution was then injected onto a Superdex 75 GL 10/300 size-exclusion chromatography column, and eluted with the buffer that would be used in the subsequent experiments at a flow rate of 0.7 ml/min (fig. 13). Fractions were collected as 500  $\mu$ l aliquots and the two aliquots corresponding to the monomer peak, eluting at approximately 15-17 mL were collected and combined. The A $\beta$  concentration

of the combined fractions was determined using UV-Vis absorbance spectroscopy, using an extinction coefficient of  $\epsilon_{280} = 1400 \text{ M}^{-1}\text{cm}^{-1}$  [66].

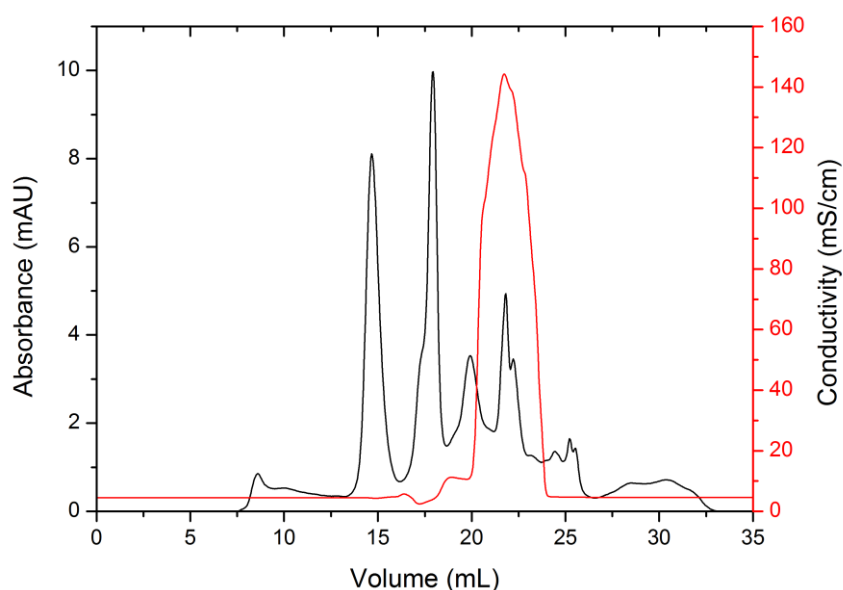


Figure 13. Chromatogram showing the purification of monomeric  $A\beta(1-42)$  using a Superdex 75 GL 10/300 size-exclusion column. The peak at ~15 mL corresponds to monomeric  $A\beta(1-42)$ . The subsequent peaks are buffer components, as indicated by the change in conductivity.

## Amyloid fibril formation controls

The quality of the purified  $A\beta$  solutions was assessed by examining the reproducibility of amyloid formation in a ThT amyloid kinetics assay and by examining the resulting fibrils by atomic force microscopy. This was typically done by diluting purified  $A\beta$  to  $5 \mu\text{M}$  concentration, followed by addition of  $1 \mu\text{M}$  ThT. The samples were distributed as at least three replicates in a 96-well microtiter plate, and the ThT fluorescence was read intermittently over 8 hours. The resulting kinetic traces replicate very well the known amyloid formation kinetics described in the theoretical section of this thesis, and also show that the variance of the reaction is low (fig. 14, left).

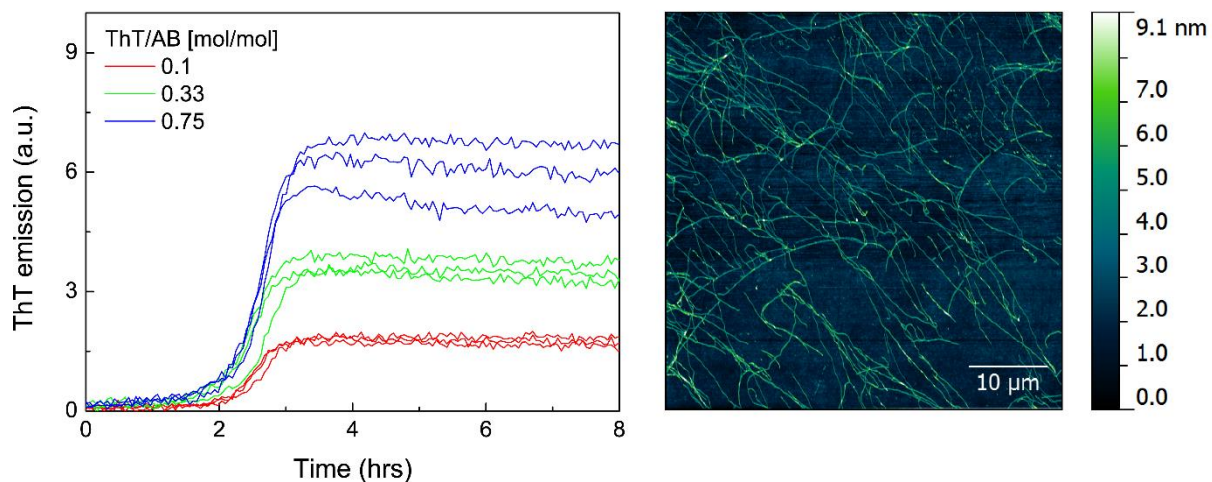


Figure 14. Left: Formation of amyloid fibrils by  $A\beta(1-42)$ , as measured by ThT fluorescence at different dye-loads. Typical sigmoidal kinetics with a distinct lag phase, a fast growth phase and a plateau phase. 3 traces of the same experiment are shown to give an indication of the reproducibility of the experimental setup. Right: AFM imaging of  $A\beta(1-42)$  deposited on a glass surface.

Further, the amyloid- $\beta$  fibrils were examined in an nTegra PRIMA AFM setup (NT-MDT) to confirm the macromolecular size and shape of the obtained fibrils (fig. 14, right).  $A\beta(1-42)$  fibrils are approximately 8-10 nm in height and range up to 10s of microns in length, a result that is in agreement with typical numbers for  $A\beta$  amyloid fibrils [68]. This confirms the establishment of a functioning protocol for expression and purification of highly monomeric  $A\beta$  protein, and the relevant assays for studying fibril formation kinetics and morphology.

# **Study I – ThT fluorescence as a tool to differentiate between amyloid fibrils**

## **Background**

The fluorescence enhancement of ThT when it interacts with amyloid fibrils is not always linearly related to the concentrations of fibrils and dye. For example, different isoforms of the same fibril can often give rise to dramatically different emission intensities for samples that are at first glance very similar. In the paper '*Steady-state and time-resolved Thioflavin-T fluorescence can report on morphological differences in amyloid fibrils formed by A $\beta$ (1-40) and A $\beta$ (1-42)*' I have investigated this heterogeneity in order to better understand how ThT functions in its capacity as an amyloid fibril probe.

## **A $\beta$ (1-40) and A $\beta$ (1-42) produces different ThT emission in concentration-matched samples**

In order to make direct quantitative comparisons between fibril samples of different A $\beta$  variants, we setup and used a bischinchonic acid assay (BCA) to estimate the protein concentration in our various samples. This procedure enabled us to match the fibril concentrations in different samples thereby making it possible to directly compare the ThT fluorescence intensities recorded. We did this by measuring the monomer concentration in the samples prior to and after fibrillisation, and could therefore also determine the typical reactions yields in the fibril forming reactions. We found that both A $\beta$ (1-40) and A $\beta$ (1-42) aggregated to a 90-95% extent (paper I, fig. S2).

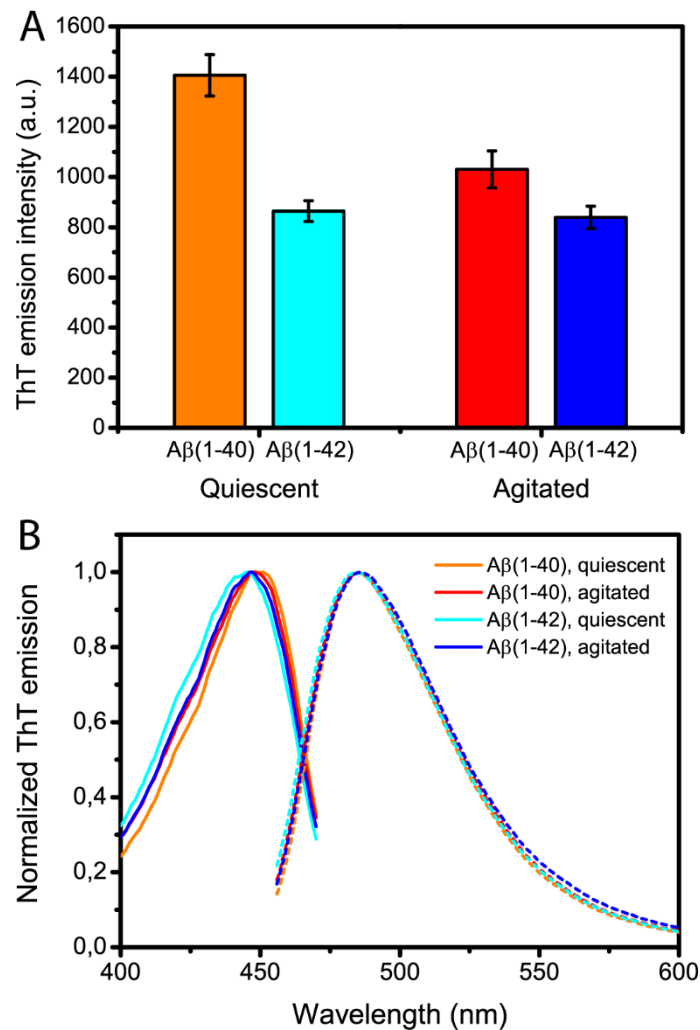


Figure 15. (A) ThT steady-state emission intensity measured in presence of A $\beta$ (1-40) or A $\beta$ (1-42) fibrils incubated at either quiescent or agitated conditions. (B) Emission and excitation spectra of the same samples as in Top.

Using the concentration-matched amyloid- $\beta$  fibril samples of A $\beta$ (1-40) and A $\beta$ (1-42), we found that the emission intensity from ThT is indeed different for different fibril variants but also for different conditions by which each fibril type was prepared (quiescent or agitated) (fig 15A). In fibrils formed under quiescent conditions, the emission intensity from A $\beta$ (1-40) is 1.7-fold stronger than that of A $\beta$ (1-42). This result suggests that there are profound differences in ThT fluorescence enhancement by fibrils formed from these two peptides, an important finding, as it reveals that variations in ThT emission intensity does not necessarily relate to variations in fibril concentration. For fibrils formed under agitated conditions, A $\beta$ (1-40) still shows stronger fluorescence enhancement, though the difference is now 1.3-fold. In general, agitation decreases the ThT fluorescence intensity, typically because the forces introduced by shaking act to increase the fibril fragmentation rate, but here we show (by AFM analysis) that it also appears to induce lateral clustering of fibrils.

## **The emission differences are explained by morphological features of A $\beta$ fibrils**

In order to investigate if these differences between A $\beta$ (1-40) and A $\beta$ (1-42) could be explained by differences in the structure and/or number of the ThT binding site(s) we measured emission and excitation spectra (fig 15B). We found no distinct differences in spectral shape indicating that the varying intensity cannot be explained by spectral change. We also measured circular dichroism spectra (paper I, fig. 3B) of the fibrils and could conclude that there are no dramatic differences in the secondary structure content of the A $\beta$ (1-40) and A $\beta$ (1-42) fibrils, at least not at a level that could explain the differences in ThT emission intensity. Therefore, to further characterise the origin of the intensity difference, time-resolved ThT fluorescence was used to determine the average excited state lifetime of ThT in its fibril-bound state. This revealed a small but distinctive and reproducible difference in the intensity-averaged fluorescence lifetime between the two fibril types. This difference was independent of the aggregation conditions, suggesting that it represents an inherent property of the A $\beta$ (1-40) and A $\beta$ (1-42) fibrils respectively. Atomic-level structural studies of A $\beta$  fibrils have indeed indicated slightly different structures for A $\beta$ (1-40) and A $\beta$ (1-42) fibrils [56], leading us to suggest that the different ThT fluorescence lifetimes represent a slight difference in the ThT binding site for the two isoforms.

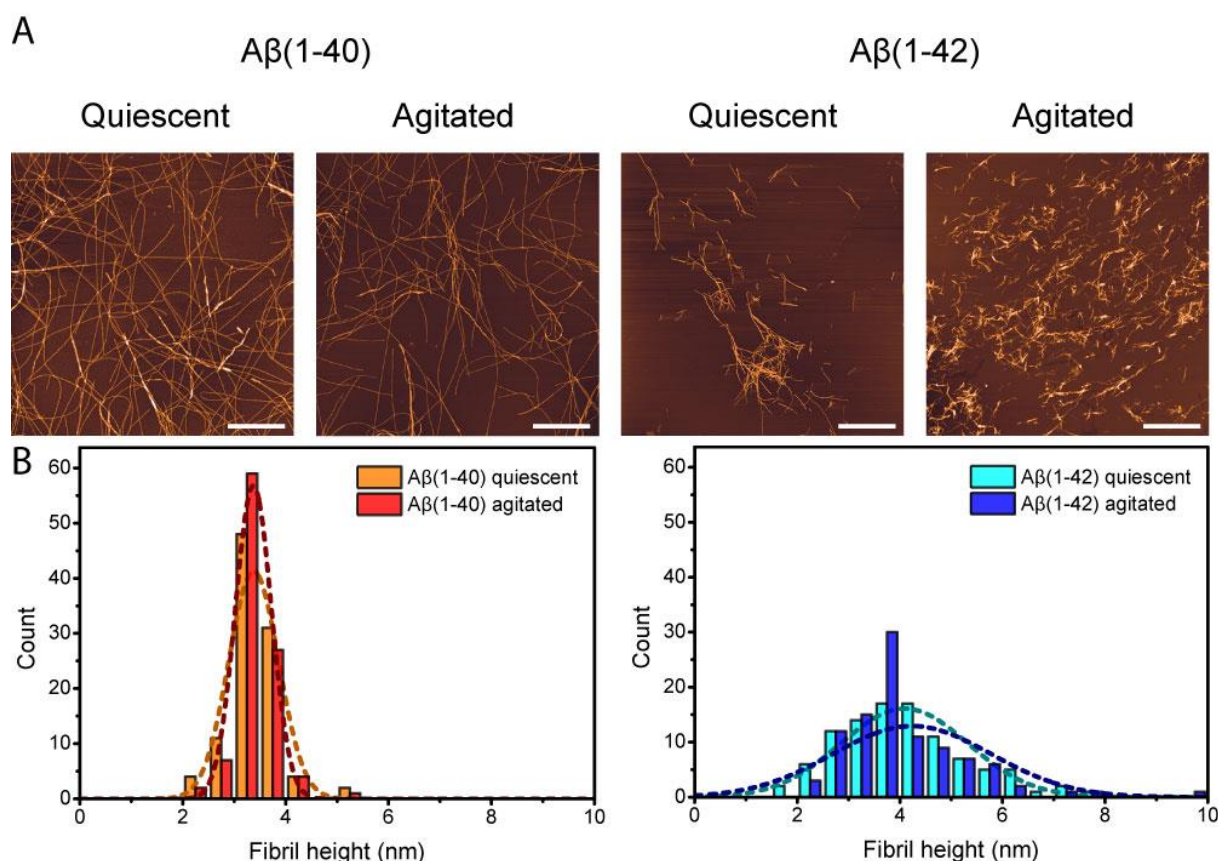


Figure 16. (A): Atomic force microscopy images of  $A\beta(1-40)$  fibrils (left panels) formed at quiescent and agitated conditions, and  $A\beta(1-42)$  fibrils (right panels) formed at quiescent and agitated conditions. (B): Histograms showing the height distributions of the same samples as in (A).

Finally we recorded AFM images of the fibril samples in order to compare their morphological features (fig. 16A). We found from height measurements of individual fibrils that the  $A\beta(1-40)$  fibrils are thinner than the  $A\beta(1-42)$  fibrils, but also that their height distribution is narrower (fig. 16B). It is also evident on a qualitative level that  $A\beta(1-40)$  fibrils are longer, at least for agitated samples, than  $A\beta(1-42)$  fibrils. This is expected, given that  $A\beta(1-42)$  has a higher rate constant for nucleation, leading to formation of more fibrils, but shorter ones. We thus concluded that  $A\beta(1-40)$  forms longer and slenderer fibrils, that also appear less laterally clustered (paper I, fig. S7), and that this morphological difference allows for higher binding capacity (more available ThT binding sites) than the shorter more clumped together  $A\beta(1-42)$  fibrils.

### Further investigation into the Th-T fluorescence lifetime

In ongoing work I am further characterising the ThT fluorescence lifetime when bound to  $A\beta$  fibrils, and present results suggesting that it is more complex than at first thought. First, the ThT fluorescence lifetime is dependent on the ratio of ThT:fibrils, as a titration of ThT into a fibrillar  $A\beta$  sample gives a decrease in the intensity-averaged lifetime of ThT (fig 17A). Conversely, the same effect is observed when  $A\beta(1-42)$  fibrils are titrated into a ThT solution

(fig 17B). The quenching of the ThT fluorescence lifetime is not a result of increased contribution of free ThT, as the emission from free ThT is too low to make a significant contribution in the time window used to record the decay. These results indicate that as the binding of ThT to A $\beta$ (1-42) fibrils is increasingly saturated, the fluorescence emission is also quenched. I am currently trying to utilise this effect to measure the formation kinetics of A $\beta$ (1-42). The quenching effect is especially pronounced at low A $\beta$ (1-42) concentrations, indicating that time-resolved ThT fluorescence has the capacity of being very sensitive for low fibril concentrations, thus making it especially useful for obtaining information in the normally unresponsive lag phase.

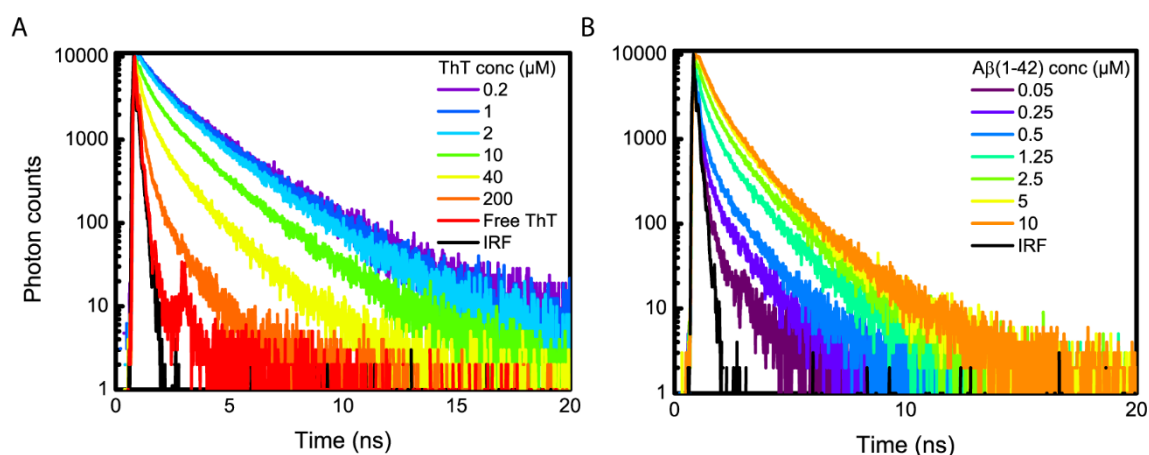


Figure 17. Fluorescence emission decay curves of: (A) increasing amounts of ThT in presence of 10  $\mu$ M A $\beta$ (1-42) fibrils. (B) increasing amounts of A $\beta$ (1-42) fibrils in presence of 10  $\mu$ M ThT.

## **Study II – YOYO-1 as a novel amyloid fibril fluorescent stain**

### **Background**

YOYO-1 (fig. 8), a homodimer derivative of oxazole yellow (YO), is a dye that is typically used to detect double-stranded DNA. Each individual YO moiety is a molecular rotor whose emission intensity is governed by its ability to rotate around the bond that connects its two aromatic ring systems [64]. It has previously been shown to interact with amyloid fibrils [69], and I wanted to expand on this study and evaluate its use as an amyloid indicator dye. The chemical structure of the individual YO moieties in YOYO-1 bears some resemblance to ThT, which sparked our initial interest of testing it as an amyloid stain; further as high binding affinity is important for molecular probes for amyloid recognition I decided to test the homodimer as it may, due to its higher overall charge display stronger binding. YOYO-1 has some inherent advantages; it has a three-fold higher extinction coefficient than ThT, it has a very high binding affinity to DNA, which I hoped would translate to amyloids, and its spectral properties overlap very well with excitation light sources and standard filters used in e.g. fluorescence microscopes and plate readers. Furthermore, it belongs to a family of homodimeric cyanine dyes that together covers a large part of the visible spectrum, thus opening up the possibility of adapting these dyes into a toolbox that would allow for versatile colour-tuning of amyloid fluorescence assays.

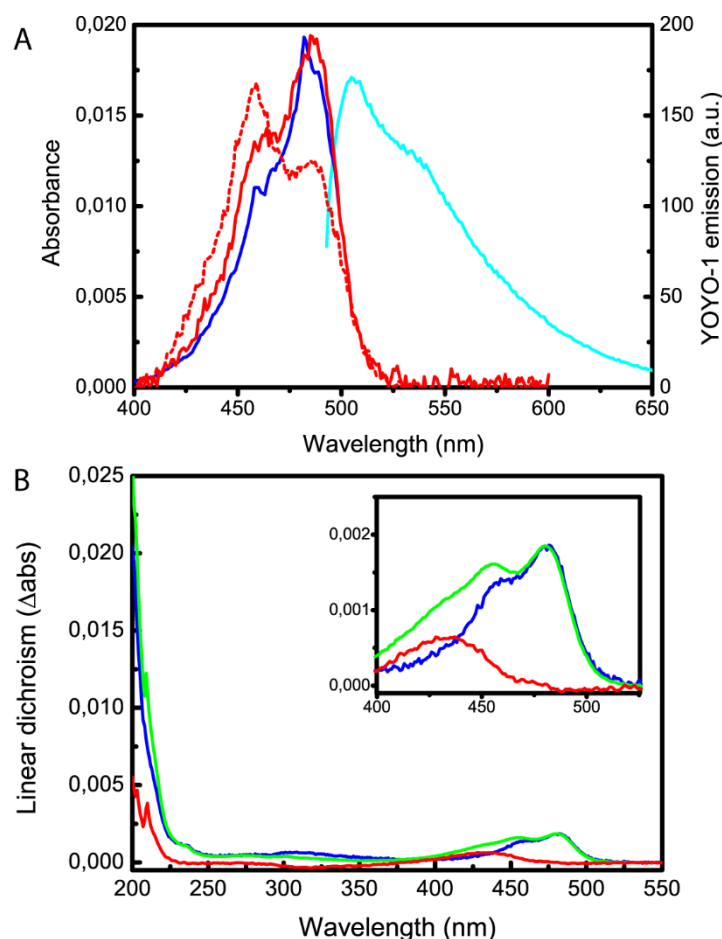


Figure 18. (A): Absorbance (red), emission (cyan) and excitation (blue) spectra of 150 nM YOYO-1 in solution (dashed line) and 150 nM YOYO-1 in presence of 5  $\mu$ M fibrillar  $A\beta(1-42)$  (solid line). (B): Linear dichroism spectra of 25  $\mu$ M fibrillar  $A\beta(1-42)$  in presence of 500 nM YOYO-1 (blue) and in presence of 500 nM YOYO-1 and 500 nM ThT (green). The red curve represents the subtraction of the YOYO-1 only LD spectrum (blue) from the YOYO-1 + ThT LD spectrum (green).

## Absorption shift and emission increase of YOYO-1 in presence of $A\beta(1-42)$

To evaluate the usefulness of YOYO-1 as an amyloid stain, I first measured the absorption and fluorescence of samples containing YOYO-1 and  $A\beta(1-42)$  amyloid fibrils. YOYO-1 has a dual-peak absorption band at 460-490 nm. These two peaks are shifted in intensity in presence of  $A\beta(1-42)$  relative to buffer solution (figure 18A, red curves), with the 490 nm peak becoming dominant relative to the 460 nm peak in the fibril-bound state. In accordance with previous studies in DNA [64], we attribute this to a conformational change of YOYO-1, from a self-stacking to a non-stacked conformation upon binding to amyloid fibrils. Fluorescence measurements revealed that the emission intensity of YOYO-1 is increased as much as 200-fold in presence of  $A\beta(1-42)$  fibrils. To characterise the binding mode of YOYO-1 to  $A\beta(1-42)$  fibrils, I measured linear dichroism spectra of  $A\beta(1-42)$  fibrils in presence of YOYO-1. The LD spectrum (fig. 18B) also shows the dual peak at 460-490 nm, with the 490 nm peak dominating, providing further confirmation that the absorption shift from 460 nm to 490 nm represents binding of YOYO-1 to  $A\beta(1-42)$  fibrils. The positive sign of the LD spectrum indicates that

YOYO-1 is bound to A $\beta$ (1-42) fibrils with its long axis parallel to the fibril axis, consistent with the binding orientation observed for thioflavin-T [39], and poly(3-thiophene acetic acid) (PTAA) [70]. Together, these results indicate that YOYO-1, like ThT, binds into groove-like ‘channels’ that are formed on the face of the amyloid fibrils by repetitions of amino acid side-chains protruding from the amyloid cross- $\beta$  core.

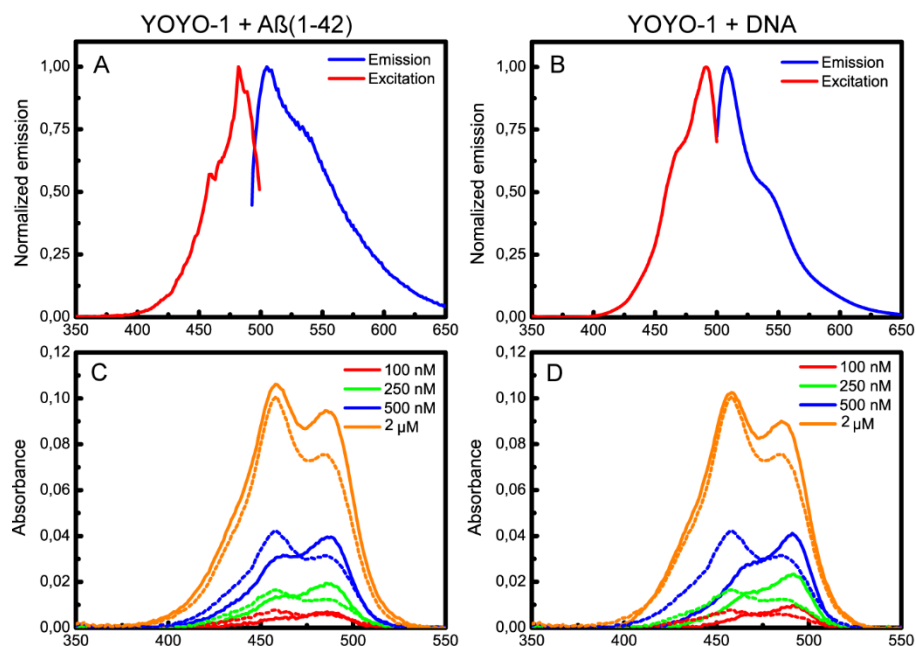


Figure 19. A and B: Emission (blue) and excitation (red) spectra of YOYO-1 in presence of (A) A $\beta$ (1-42) fibrils or (B) ct-DNA. C and D: Absorbance spectra of increasing amounts of YOYO-1 in presence of (C) A $\beta$ (1-42) fibrils or (D) ct-DNA.

## Comparison of YOYO-1 amyloid fluorescence to YOYO-1 DNA fluorescence

Next, I compared the emission and absorption of YOYO-1 in presence of amyloid to that of YOYO-1 in presence of double-stranded DNA (fig 19). I found that both the excitation and emission spectrum are very similar in the two cases (fig 19A and 19B), indicating that the physico-chemical environment of amyloid-bound YOYO-1 is similar as in double-stranded DNA. The fold-increase of YOYO-1 is higher when bound to DNA [65], which we attribute to intercalation. YOYO-1 is known to intercalate in double-stranded DNA, leading to a strongly stabilized ring system, whereas the proposed groove-like binding in amyloid fibrils likely results in lesser stabilisation. The absorption shift from 460 nm to 490 nm also seems to mimic DNA (fig 19C and 19D), with a regrowth of the 460 nm peak at high dye-loads, indicating a saturation of the binding. This saturation is not seen for ThT (paper II, fig. 3), indicating that the binding affinity for A $\beta$ (1-42) fibrils of YOYO-1 is stronger than that of ThT, possibly a reflection of its stronger electrostatic attraction.

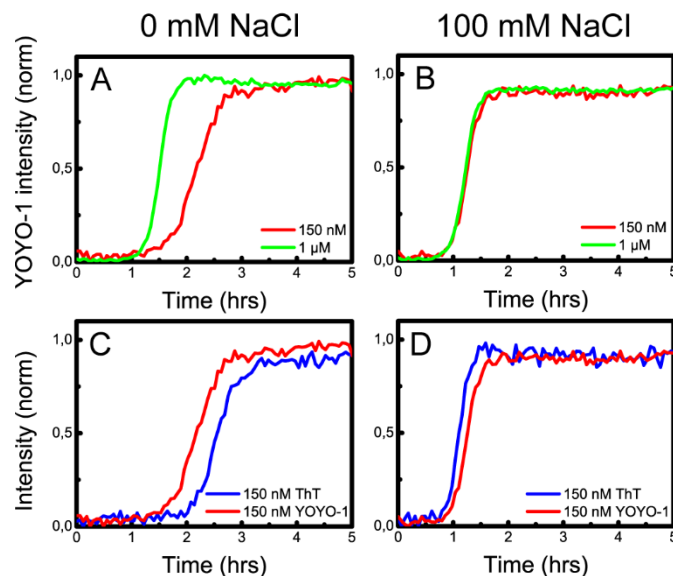


Figure 20. Amyloid formation by  $A\beta(1-42)$  monitored by YOYO-1 and ThT fluorescence. **Top rows:** Change in YOYO-1 fluorescence as a function of time upon  $A\beta(1-42)$  aggregation. Kinetic data were recorded in phosphate buffers containing (A) 0 mM sodium chloride and (B) 100 mM sodium chloride. The total  $A\beta(1-42)$  concentration in each sample was 5  $\mu\text{M}$ . The YOYO-1 concentrations are indicated in the figure legends. **Bottom rows:** Comparison of the change in YOYO-1 fluorescence (red curves) and ThT fluorescence (blue curves) as function of time upon  $A\beta(1-42)$  aggregation. Kinetic data were recorded in phosphate buffers containing (C) 0 mM sodium chloride and (D) 100 mM sodium chloride. The total  $A\beta(1-42)$  concentration in each sample was 5  $\mu\text{M}$  and the dye concentration was 150 nM.

### YOYO-1 as a probe for amyloid formation kinetics

Finally, I examined the use of YOYO-1 as an amyloid indicator in kinetics measurements. I found that although YOYO-1 responds to and reports on fibril formation, it has, under some experimental conditions, a concentration dependent effect on the amyloid formation rate (fig 20A), this is not typically seen for ThT (paper II, fig. S5). It also has a rate-increasing effect compared to ThT at equimolar concentrations (fig 20C). This rate-increasing effect is, however, eliminated by addition of 100 mM NaCl (fig 20B and 20D), probably due to electrostatic screening of the strong positive charge (+4) of YOYO-1. The positive charge of YOYO-1 could act to attract negatively charged  $A\beta(1-42)$  monomers to the forming fibrils, thereby increasing both the nucleation and elongation rate. Similar effects have been observed for naturally occurring multivalent cations such as spermine and putrescine [71].

## Summary and Outlook

This thesis details the development of laboratory methods, specifically use of fluorescent dyes, to produce and characterise amyloid- $\beta$  fibrils.

I have shown how ThT fluorescence is a considerably more complex tool than what is appreciated in its standard application and my results explain why it is difficult to relate its intensity directly to fibril content. However, my work also shows how careful sample preparation and carefully chosen experimental setups makes it possible to utilise this effect, allowing for differentiation between amyloid fibrils in a way that is related to their morphological appearance. There are also promising indications that the time-resolved ThT fluorescence can become an important tool to study formation of A $\beta$  fibrils, as the ThT fluorescence lifetime is indirectly dependent on the fibril mass, and possibly also on their aggregation state.

Further, I have provided a biophysical characterisation of the amyloid-binding properties of YOYO-1, a classic DNA-binding fluorophore. YOYO-1 emission exhibits a 200-fold increase in presence of amyloid- $\beta$  fibrils, coupled with absorbance shifts related to a stacking to non-stacking conformational change. YOYO-1 also exhibits linear dichroism in presence of amyloid- $\beta$  fibrils, which not only confirms the binding, but also demonstrates that YOYO-1 binds parallel to the fibril axis, analogously to the classic stain ThT. As YOYO-1 belongs to a family of homodimeric cyanine fluorophores, it provides a novel set of amyloid-binding dyes that can be used to colour-tune amyloid fluorescence to a large range of the visible spectrum.

Both of these studies relate to the interaction of small molecules with the amyloid cross- $\beta$  surface. They stand as further proof of the presence of groove-like channels on the surface of amyloid fibrils that provide binding sites for elongated molecules such as ThT or YOYO-1. Recent studies have shown that the fibril surface is of great importance for fibril elongation rates as secondary nucleation processes in amyloid forming reactions appear dependent on the fibril surface and hence possibly on the structural motif that encompass the groove-like channels. This interesting mechanic of the amyloid forming reaction is especially interesting with respect to the ability of such species to transfer and proliferate throughout the AD brain [51,72-74].

I have also described the setup of a protocol for expression and purification of A $\beta$ (1-42) for amyloid formation kinetics experiments. As a result, I have now established a diverse toolbox consisting of specialised fluorescence methods in combination with a production system for highly monomeric, seed-free A $\beta$ (1-42), enabling studies of how biological components such as lipid membranes modulate the formation of amyloid fibrils and such studies are currently underway. The results that I have obtained so far indicate that lipid vesicles increase the rate of fibril formation, and I hope to utilise the methods developed here to investigate how the presence of lipids affects the structure and morphology of amyloid fibrils, and how these features relate to their neurotoxic properties.

## Acknowledgements

I want to thank first and foremost my supervisor Elin Esbjörner Winters. You are a fantastic help and inspiration to me, and I could not have asked for a better supervisor. Some might say that a prospective PhD student should try to find a perfect supervisor, instead of a perfect project. I like to think that I got the best of both, but if we're to be true here, you chose me rather than the other way around. I am very grateful for that, and without your never-ending encouragement, sharp analytical mind and experience of the academic world, I would not have written this. Thank you.

To Bo Albinsson, part for being my co-supervisor and examiner, but also for providing a healthy (if at times somewhat blunt...) critical discussion of both scientific, academic, and completely unrelated topics. Your deep knowledge in spectroscopy has been very helpful over these few years.

To all of my other co-authors, Moa Sandberg Wranne, Mélina Gilbert Gatty and Fredrik Westerlund. Thank you for being part of this journey, I hope we will work together again in the near future.

To what has nowadays become the Esbjörner research group. Emelie, you are a very talented researcher, and a fantastic addition to what is now an actual group!

To the students that have passed through our lab during various courses and thesis projects; Moa Sandberg Wranne, Emelie Lindahl Wesén, Vilhelm Müller, Lisa Rundblad, Elin Sundin, Eneas Schmidt, Emelie Svensson, Jessy Nassif, Matilde Bengtsson, Johan Björkeröth, Carl Malina and Julia Gutman. I am certain that a great deal of you will go on to form your own academic careers (some of you are already well on your way!)

To Sara Linse and Birgitta Frohm at Lund University, and to Henrik Biverstål at Karolinska Institutet, for helping me setting up the expression and purification of amyloid- $\beta$  here at Chalmers. After many ups and downs it's finally working, and your help has been invaluable.

To my room-mates, present and former; Martin Hammarsson, Maxim Kogan, Jelena Lovric and Jens Nordmark.

To all the rest of the floor 5 colleagues (special mentions to Magnus Bälter and Vilhelm Müller for taking the time to be the opponents of this thesis). There is a certain attitude of friendship and fellowship here that I don't think will change, despite us being a part of another new institution. No better love than that between siblings, right?

Lastly, a few words for my friends, my family, and my love, Elin Bernson. You make me a better person, you encourage me when I fall, and you appreciate me when I stand. My deepest thanks.

## References

- [1] A. Alzheimer, R.A. Stelzmann, H.N. Schnitzlein, et al., An English translation of Alzheimer's 1907 paper, "Über eine eigenartige Erkrankung der Hirnrinde", *Clin. Anat.* 8 (1995) 429-431.
- [2] H. Braak, E. Braak, Neuropathological Staging of Alzheimer-Related Changes, *Acta Neuropathol. (Berl)*. 82 (1991) 239-259.
- [3] G.G. Glenner, C.W. Wong, Alzheimer's disease: initial report of the purification and characterization of a novel cerebrovascular amyloid protein, *Biochem. Biophys. Res. Commun.* 120 (1984) 885-890.
- [4] C.L. Masters, G. Simms, N.A. Weinman, et al., Amyloid plaque core protein in Alzheimer disease and Down syndrome, *Proc. Natl. Acad. Sci. U. S. A.* 82 (1985) 4245-4249.
- [5] D.J. Selkoe, The molecular pathology of Alzheimer's disease, *Neuron* 6 (1991) 487-498.
- [6] J. Hardy, D. Allsop, Amyloid deposition as the central event in the aetiology of Alzheimer's disease, *Trends Pharmacol. Sci.* 12 (1991) 383-388.
- [7] J.A. Hardy, G.A. Higgins, Alzheimer's disease: the amyloid cascade hypothesis, *Science* 256 (1992) 184-185.
- [8] E.M. Mandelkow, E. Mandelkow, Tau in Alzheimer's disease, *Trends Cell Biol.* 8 (1998) 425-427.
- [9] W.H. Organization, The world health report 2003: shaping the future, World Health Organization, 2003.
- [10] C.P. Ferri, M. Prince, C. Brayne, et al., Global prevalence of dementia: a Delphi consensus study, *Lancet* 366 (2005) 2112-2117.
- [11] A. Comas-Herrera, R. Wittenberg, L. Pickard, et al., Cognitive impairment in older people: future demand for long-term care services and the associated costs, *Int. J. Geriatr. Psychiatry* 22 (2007) 1037-1045.
- [12] K.M. Langa, M.E. Chernew, M.U. Kabeto, et al., National estimates of the quantity and cost of informal caregiving for the elderly with dementia, *J. Gen. Intern. Med.* 16 (2001) 770-778.
- [13] C. Haass, B. De Strooper, Review: Neurobiology - The presenilins in Alzheimer's disease - Proteolysis holds the key, *Science* 286 (1999) 916-919.
- [14] D. Schenk, M. Hagen, P. Seubert, Current progress in beta-amyloid immunotherapy, *Curr. Opin. Immunol.* 16 (2004) 599-606.
- [15] K. Blennow, M.J. de Leon, H. Zetterberg, Alzheimer's disease, *Lancet* 368 (2006) 387-403.
- [16] D.L. Sparks, S.W. Scheff, J.C. Hunsaker, et al., Induction of Alzheimer-Like Beta-Amyloid Immunoreactivity in the Brains of Rabbits with Dietary-Cholesterol, *Exp. Neurol.* 126 (1994) 88-94.
- [17] J.L. Eriksen, S.A. Sagi, T.E. Smith, et al., NSAIDs and enantiomers of flurbiprofen target gamma-secretase and lower A beta 42 in vivo, *J. Clin. Invest.* 112 (2003) 440-449.
- [18] M.J. Engelhart, M.I. Geerlings, A. Ruitenbergh, et al., Dietary intake of antioxidants and risk of Alzheimer disease, *J. Am. Med. Assoc.* 287 (2002) 3223-3229.
- [19] S.H. Choi, Y.H. Kim, M. Hebisch, et al., A three-dimensional human neural cell culture model of Alzheimer's disease, *Nature* 515 (2014) 274-U293.
- [20] J. Kang, H.G. Lemaire, A. Unterbeck, et al., The Precursor of Alzheimers-Disease Amyloid-A4 Protein Resembles a Cell-Surface Receptor, *Nature* 325 (1987) 733-736.
- [21] J.A. Duce, A.I. Bush, Biological metals and Alzheimer's disease: Implications for therapeutics and diagnostics, *Prog. Neurobiol.* 92 (2010) 1-18.

- [22] C. Priller, T. Bauer, G. Mitteregger, et al., Synapse formation and function is modulated by the amyloid precursor protein, *J. Neurosci.* 26 (2006) 7212-7221.
- [23] H. Mori, K. Takio, M. Ogawara, et al., Mass-Spectrometry of Purified Amyloid-Beta Protein in Alzheimers-Disease, *J. Biol. Chem.* 267 (1992) 17082-17086.
- [24] A.E. Roher, J.D. Lowenson, S. Clarke, et al., Structural Alterations in the Peptide Backbone of Beta-Amyloid Core Protein May Account for Its Deposition and Stability in Alzheimers-Disease, *J. Biol. Chem.* 268 (1993) 3072-3083.
- [25] C. Haass, M.G. Schlossmacher, A.Y. Hung, et al., Amyloid Beta-Peptide Is Produced by Cultured-Cells during Normal Metabolism, *Nature* 359 (1992) 322-325.
- [26] K.G. Mawuenyega, W. Sigurdson, V. Ovod, et al., Decreased clearance of CNS beta-amyloid in Alzheimer's disease, *Science* 330 (2010) 1774.
- [27] P.M. Douglas, A. Dillin, Protein homeostasis and aging in neurodegeneration, *J. Cell Biol.* 190 (2010) 719-729.
- [28] H. Braak, E. Braak, Frequency of stages of Alzheimer-related lesions in different age categories, *Neurobiol. Aging* 18 (1997) 351-357.
- [29] C.M. Dobson, Protein folding and misfolding, *Nature* 426 (2003) 884-890.
- [30] F. Chiti, C.M. Dobson, Protein misfolding, functional amyloid, and human disease, *Annu. Rev. Biochem.* 75 (2006) 333-366.
- [31] J.D. Sipe, A.S. Cohen, Review: History of the amyloid fibril, *J. Struct. Biol.* 130 (2000) 88-98.
- [32] D. Eisenberg, M. Jucker, The Amyloid State of Proteins in Human Diseases, *Cell* 148 (2012) 1188-1203.
- [33] E. Gazit, Self-assembled peptide nanostructures: the design of molecular building blocks and their technological utilization, *Chem. Soc. Rev.* 36 (2007) 1263-1269.
- [34] R. Nelson, M.R. Sawaya, M. Balbirnie, et al., Structure of the cross-beta spine of amyloid-like fibrils, *Nature* 435 (2005) 773-778.
- [35] K.E. Marshall, K.L. Morris, D. Charlton, et al., Hydrophobic, Aromatic, and Electrostatic Interactions Play a Central Role in Amyloid Fibril Formation and Stability, *Biochemistry* 50 (2011) 2061-2071.
- [36] P. Marek, A. Abedini, B.B. Song, et al., Aromatic interactions are not required for amyloid fibril formation by islet amyloid polypeptide but do influence the rate of fibril formation and fibril morphology, *Biochemistry* 46 (2007) 3255-3261.
- [37] A.W.P. Fitzpatrick, G.T. Debelouchina, M.J. Bayro, et al., Atomic structure and hierarchical assembly of a cross-beta amyloid fibril, *Proc. Natl. Acad. Sci. U. S. A.* 110 (2013) 5468-5473.
- [38] E.D. Eanes, G.G. Glenner, X-Ray Diffraction Studies on Amyloid Filaments, *J. Histochem. Cytochem.* 16 (1968) 673-&.
- [39] A.K. Buell, E.K. Esbjorner, P.J. Riss, et al., Probing small molecule binding to amyloid fibrils, *PCCP* 13 (2011) 20044-20052.
- [40] M.R.H. Krebs, E.H.C. Bromley, A.M. Donald, The binding of thioflavin-T to amyloid fibrils: localisation and implications, *J. Struct. Biol.* 149 (2005) 30-37.
- [41] T. Luhrs, C. Ritter, M. Adrian, et al., 3D structure of Alzheimer's amyloid-beta(1-42) fibrils, *Proc. Natl. Acad. Sci. U. S. A.* 102 (2005) 17342-17347.
- [42] H. Puchtler, F. Sweat, M. Levine, On Binding of Congo Red by Amyloid, *J. Histochem. Cytochem.* 10 (1962) 355-&.

- [43] A.I. Sulatskaya, A.A. Maskevich, I.M. Kuznetsova, et al., Fluorescence Quantum Yield of Thioflavin T in Rigid Isotropic Solution and Incorporated into the Amyloid Fibrils, *PLoS One* 5 (2010).
- [44] J. Hardy, D.J. Selkoe, *Medicine - The amyloid hypothesis of Alzheimer's disease: Progress and problems on the road to therapeutics*, *Science* 297 (2002) 353-356.
- [45] D.M. Walsh, I. Klyubin, J.V. Fadeeva, et al., Amyloid-beta oligomers: their production, toxicity and therapeutic inhibition, *Biochem. Soc. Trans.* 30 (2002) 552-557.
- [46] B. Bolognesi, J.R. Kumita, T.P. Barros, et al., ANS binding reveals common features of cytotoxic amyloid species, *ACS Chem. Biol.* 5 (2010) 735-740.
- [47] R. Crespo, F.A. Rocha, A.M. Damas, et al., A Generic Crystallization-like Model That Describes the Kinetics of Amyloid Fibril Formation, *J. Biol. Chem.* 287 (2012) 30585-30594.
- [48] T.P.J. Knowles, C.A. Waudby, G.L. Devlin, et al., An Analytical Solution to the Kinetics of Breakable Filament Assembly, *Science* 326 (2009) 1533-1537.
- [49] A. Lomakin, D.B. Teplow, D.A. Kirschner, et al., Kinetic theory of fibrillogenesis of amyloid beta-protein, *Proc. Natl. Acad. Sci. U. S. A.* 94 (1997) 7942-7947.
- [50] G. Tian, F. Simona, R.A. Broglia, et al., Thermodynamics of beta-amyloid fibril formation, *J. Chem. Phys.* 120 (2004) 8307-8317.
- [51] S.I. Cohen, S. Linse, L.M. Luheshi, et al., Proliferation of amyloid-beta<sub>42</sub> aggregates occurs through a secondary nucleation mechanism, *Proc. Natl. Acad. Sci. U. S. A.* 110 (2013) 9758-9763.
- [52] L. Nielsen, R. Khurana, A. Coats, et al., Effect of environmental factors on the kinetics of insulin fibril formation: elucidation of the molecular mechanism, *Biochemistry* 40 (2001) 6036-6046.
- [53] S.R. Collins, A. Dougllass, R.D. Vale, et al., Mechanism of prion propagation: Amyloid growth occurs by monomer addition, *PLoS Biol.* 2 (2004) 1582-1590.
- [54] S.I.A. Cohen, M. Vendruscolo, C.M. Dobson, et al., Nucleated polymerization with secondary pathways. III. Equilibrium behavior and oligomer populations, *J. Chem. Phys.* 135 (2011).
- [55] R. Tycko, Molecular structure of amyloid fibrils: insights from solid-state NMR, *Q. Rev. Biophys.* 39 (2006) 1-55.
- [56] M. Fandrich, M. Schmidt, N. Grigorieff, Recent progress in understanding Alzheimer's beta-amyloid structures, *Trends Biochem. Sci.* 36 (2011) 338-345.
- [57] R. Tycko, R.B. Wickner, Molecular Structures of Amyloid and Prion Fibrils: Consensus versus Controversy, *Acc. Chem. Res.* 46 (2013) 1487-1496.
- [58] J.R. Lakowicz, *Principles of fluorescence spectroscopy*, Springer Science & Business Media, 2013.
- [59] R.Y. Tsien, The green fluorescent protein, *Annu. Rev. Biochem.* 67 (1998) 509-544.
- [60] H. Levine, Thioflavine-T Interaction with Synthetic Alzheimer's-Disease Beta-Amyloid Peptides - Detection of Amyloid Aggregation in Solution, *Protein Sci.* 2 (1993) 404-410.
- [61] M. Biancalana, S. Koide, Molecular mechanism of Thioflavin-T binding to amyloid fibrils, *Biochim. Biophys. Acta: Proteins Proteomics* 1804 (2010) 1405-1412.
- [62] M. Groenning, Binding mode of Thioflavin T and other molecular probes in the context of amyloid fibrils-current status, *J. Chem. Biol.* 3 (2010) 1-18.
- [63] M. Canete, A. Villanueva, A. Juarranz, et al., A study of interaction of thioflavine T with DNA: evidence for intercalation, *Cell. Mol. Biol.* 33 (1987) 191-199.

- [64] C. Carlsson, A. Larsson, M. Jonsson, et al., Optical and Photophysical Properties of the Oxazole Yellow DNA Probes Yo and Yoyo, *J. Phys. Chem.* 98 (1994) 10313-10321.
- [65] A.N. Glazer, H.S. Rye, Stable Dye-DNA Intercalation Complexes as Reagents for High-Sensitivity Fluorescence Detection, *Nature* 359 (1992) 859-861.
- [66] D.M. Walsh, E. Thulin, A.M. Minogue, et al., A facile method for expression and purification of the Alzheimer's disease-associated amyloid beta-peptide, *FEBS J.* 276 (2009) 1266-1281.
- [67] F.W. Studier, Protein production by auto-induction in high-density shaking cultures, *Protein Expression Purif.* 41 (2005) 207-234.
- [68] R. Khurana, C. Ionescu-Zanetti, M. Pope, et al., A general model for amyloid fibril assembly based on morphological studies using atomic force microscopy, *Biophys. J.* 85 (2003) 1135-1144.
- [69] S. Stefansson, D.L. Adams, C.-M. Tang, Fluorescence assays, *BioTechniques*.
- [70] J. Wiggenius, M.R. Andersson, E.K. Esbjorner, et al., Interactions between a luminescent conjugated polyelectrolyte and amyloid fibrils investigated with flow linear dichroism spectroscopy, *Biochem. Biophys. Res. Commun.* 408 (2011) 115-119.
- [71] J. Luo, C.H. Yu, H. Yu, et al., Cellular polyamines promote amyloid-beta (A $\beta$ ) peptide fibrillation and modulate the aggregation pathways, *ACS Chem. Neurosci.* 4 (2013) 454-462.
- [72] B. Bolognesi, S.I.A. Cohen, P.A. Terol, et al., Single Point Mutations Induce a Switch in the Molecular Mechanism of the Aggregation of the Alzheimer's Disease Associated A $\beta$ (42) Peptide, *ACS Chem. Biol.* 9 (2014) 378-382.
- [73] G. Meisl, X.T. Yang, E. Hellstrand, et al., Differences in nucleation behavior underlie the contrasting aggregation kinetics of the A $\beta$  40 and A $\beta$  42 peptides, *Proc. Natl. Acad. Sci. U. S. A.* 111 (2014) 9384-9389.
- [74] S.I. Cohen, P. Arosio, J. Presto, et al., A molecular chaperone breaks the catalytic cycle that generates toxic A $\beta$  oligomers, *Nat. Struct. Mol. Biol.* 22 (2015) 207-213.